DETECTION OF WINDING DEFORMATION IN POWER TRANSFORMERS

A Thesis Submitted in Partial Fulfillment of the Requirements for the Award of the Degree of Master of Technology

in

Electrical Engineering

(Power, Control & Drives)

By:

Saroja Kanti Sahoo

Roll No. 211ee2138

DEPARTMENT OF ELECTRICAL ENGINEERING

NATIONAL INSTITUTE OF TECHNOLOGY, ROURKELA

PIN-769008, ODISHA

(2011-2013)

DETECTION OF WINDING DEFORMATION IN POWER TRANSFORMERS

A Thesis Submitted in Partial Fulfillment of the Requirements for the Award of the Degree of Master of Technology

in

Electrical Engineering

(Power, Control & Drives)

By

Saroja Kanti Sahoo

Under the Supervision of

Dr. S. Gopalakrishna

DEPARTMENT OF ELECTRICAL ENGINEERING

NATIONAL INSTITUTE OF TECHNOLOGY, ROURKELA

PIN-769008, ODISHA

(2011-2013)

To

God and my parents

National Institute Of Technology, Rourkela

Certificate

This is to certify that the thesis entitled **"Detection Of Winding Deformation In Power Transformers"** submitted by **Ms. Saroja Kanti Sahoo** to the National Institute of Technology, Rourkela for the award of degree of **Masters of technology** in **Electrical Engineering** of specialization**, Power, Control and Drives,** is a bonafide record of research carried out by her under my supervision. The content of this thesis, in full or in parts, have not been submitted to any other Institute or University for the award of any degree or diploma.

Date:

Place:

Dr. S. Gopalakrishna
Assistant Professor
Department of Electrical Engineering
National Institute of Technology, Rourkela
769008

ACKNOWLEDGEMENT

I would like to offer my humble salutations to the supreme lord for giving me the creative energy, intellect and patience to complete this project work successfully. I wish to express my gratitude and sincere thanks to my supervisor, "**Dr. S. Gopalakrishna**", **Department of Electrical Engineering**, for his constant encouragement, guidance and support. His ideas and suggestions were helpful for timely accomplishment of the target aimed.

Further, I would like to thank **Prof. A. K. Panda, Head of the department**, and all the faculties of Electrical Engineering department for their valuable suggestions and comments for improvement at each stage of the research work.

I wish to express my gratitude towards my parents, for keeping faith in my abilities and encouraging me to improve at every step. I am grateful to my elder sister for inspiring me to work hard and to keep patience throughout the work. I would like to thank my younger brother who helped me to think logically every problem and stay calm to reach a solution. Last but not the least, I am thankful to my friends who helped me forget my worries and have a relaxed mind.

Saroja Kanti Sahoo

ABSTRACT

Power transformers are the most expensive and critical component of our power system. Its failure would be a costly event. Winding deformation is caused mainly due to short circuit events, other reasons may be ageing of insulation, and mechanical stresses developed due to transportation. Although, deformation may not result in immediate failure, however the dielectric strength of the winding is greatly reduced. And a further untoward short circuit faults may result in complete rupture of insulation which will result in complete damage of the winding. To prevent permanent damage of the transformers, a routine diagnosis is necessary for detection of winding deformation.

Among all the diagnostic approaches, sweep frequency response analysis (SFRA) is a powerful and highly sensitive diagnostic method. In this work, for the purpose of analysis of deformation on the transformer winding, a benchmark winding is considered which has already been validated for experimental studies. It is found from the comparison of 10 and 20 section models on the basis of accuracy, number of resonant frequencies required, and transfer function computation and complexity that the optimal model is the 10 section model.

The winding is modeled using finite element method (FEM) based software and parameters such as capacitance and inductance are calculated for 10 section healthy coil. Using these parameter values, SFRA plots are obtained which are a set of reference for deformation analysis. The winding is modeled as radially and axially deformed coils using FEM software. The parameters change with deformation in the winding. The deformation is carried at five consecutive sections, and affected parameters are calculated for the same. The main purpose of doing so is to find the location of deformation corresponding to a similar deformation in an actual transformer. The main advantage of the FEM modeling is we can deform the sections as desired unlike in an actual case and obtain the fingerprint graphs from the modified parameter values. The SFRA plots are obtained for the deformations at five sections for axial and radial deformations. A comparison is carried between the SFRA plots for deformed cases with the reference set. The deviations observed are in resonant frequencies, peak current magnitude and bandwidth. From the observations, the type and location of deformation can be found corresponding to a similar deformation in an actual transformer.

TABLE OF CONTENTS

LIST OF FIGURES

LIST OF TABLES

LIST OF SYMBOLS

B	Flux density vector
B_x	Radial flux density
B_y	Axial flux density
J	Current density vector
F_x	Radial force
F_y	Axial force
NI	Ampere turns
μ_o	Absolute permeability
B_{gp}	Air gap flux density
H_w	Winding height in meters
Z_{pu}	Per unit impedance
S	Rated power in MVA
f	frequency
I_{hv}	Current in the HV winding
I_{lv}	Current in the LV winding
V_l	Voltage across LV winding
V_l'	Voltage across HV winding
R_s	Series resistance between adjacent sections of helical coil
R_g	Resistance between section and ground
C_g	Capacitance between section and ground
L_{ii}	Self-inductance of i^{th} section
M_{i-j}	Mutual inductance between $i^{th}$and j^{th} section of the coil
acc_n	Percentage of deviation from measured value for n^{th}section
H	Harmonic order
m	Measured value
f_n	Resonant and anti-resonant frequencies for n^{th} section
f_o	Resonant frequency in kHz
$\lvert\Delta f_o\rvert\%$	Percentage of deviation in resonant frequency from reference set

I_o	Peak input current
$\|\Delta I_o\|\%$	Percentage of deviation in Peak input current from reference set
B.W.	Bandwidth in kHz
$\|\Delta$ B.W.$\|\%$	Percentage of deviation in bandwidth in kHz

ABBREVIATIONS

FRA	Frequency Response Analysis
LVI	Low Voltage Impulse
SFRA	Sweep Frequency Response Analysis
FEM	Finite Element Method

CHAPTER 1

INTRODUCTION

1.1. Overview
1.2. Detection of winding deformation techniques
1.3. Literature review
1.4. Motivation
1.5. Objectives
1.6. Thesis Layout

1.1. Introduction

Power transformers are the most expensive and important component in a high voltage electric power system. They are generally involved in energy transfer in power transmission and distribution networks, converting ac voltage or current from one level to another level depending on the receiver end. During its lifetime, it is subjected to mainly electrical, mechanical and thermal stresses. The main reason behind the stresses can be due to ageing of insulation, during transportation, and the most critical reason is a short circuit event. During short circuit, the current in the transformer winding is enormous as compared to normal current. The high magnitude of short circuit current has detrimental effect on the transformer and other equipments associated with it.

The interaction of short circuit current and the mutual flux (linking both the primary and secondary windings of transformer) gives rise to large amount of electromagnetic forces which are responsible for the deformations occurring in the transformer winding. The winding is subjected to mainly two types of deformations, axial deformation due to the action of axial force and radial deformation due to the action of radial forces on it. The deformations in the winding may lead to permanent failure of the transformer, if undiagnosed for long period of time. The short circuit withstand capability is drastically reduced due to deformation in the winding. Future short circuit faults and high mechanical or dielectric stress may completely rupture the insulation and may result in permanent damage of the transformer. Since, the failure of a transformer will be dangerous and costly for the utility, proper diagnosis is necessary to prevent its overall collapse. Sweep frequency response analysis is a recent popular diagnostic approach because of its sensitive nature.

1.2. DETECTION OF WINDING DEFORMATION

Commonly used diagnostic techniques are:

1. **Reactance Comparison Method**: In this method, the reactance of the transformer under test is measured before and after a short circuit test. According to IEC-60075 standard, the reactance should not exceed 1% for 100 MVA and above rated power transformers. However, this method is not applicable for detecting winding displacements which has negligible impact on the reactance.

2. **Frequency Response Analysis (FRA):** FRA is a powerful diagnostic technique and is based on the principle that every transformer has its unique signature. FRA signature is the transfer function output/input for an entire range of frequency starting from few Hz to MHz of a transformer. The signature can be obtained either by injecting an impulse across the transformer terminals at low voltages, or by making a frequency sweep of a sinusoidal signal. The former approach is known as low voltage impulse (LVI) method and the latter is sweep frequency response analysis (**SFRA**). The obtained measurements are compared with a reference set. The reference can be a previous measurement during healthy condition in time based comparison. While if the references are drawn from separately tested legs of transformer, such comparison is known as construction based comparison. The comparison done with identically constructed transformer is known as type based comparison. If the comparisons show deviations in the nature of the curves, it indicates deformation or displacement of the winding.

   SFRA is a powerful and highly sensitive technique. The main advantages of **SFRA** over LVI are:

   - High Signal to noise ratio because of the filtering of the broadband noise by the network analyzer.
   - Less measuring equipment needed for the purpose
   - Finer frequency resolution can be achieved even at low frequencies which was not possible in LVI approach.
   - Wider range of frequencies can be injected.

1.3. Literature Review

Although power transformers are found to be reliable during their service, they are subjected to breakdowns due to frequent short circuits [9]. The short circuit withstand capability is reduced d after an initial occurrence of short circuit, as a result even a minor mechanical stress with due course of time will prove to be fatal to transformer's life. The electromagnetic forces developed due to the short circuit result in the deformation of the transformer windings. The effect of axial and radial forces are tilting, spiraling of conductors, bending between the radial spacers, forced and free buckling of the conductors. As the electromagnetic forces are proportional to the square of the current, they become dangerous when a short-circuit occurs,

either in the system supplied by the transformer or especially inside the transformer itself [3, 11]. Proper diagnosis of winding deformation is essential to prevent damage and failure of transformers and disruption of smooth operation. Earlier low voltage impulse (LVI) was a widely used diagnosis approach. The first application of LVI was made in Poland in 1966 [6].

The first major breakthrough in the field of research was in the year 1978 when for the first time frequency response analysis approach was added and identified as a much better alternative to LVI [15]. The disadvantages of LVI are that it is subjected to interference effects and extensive calibration procedures [15], further FRA increased the sensitivity of detecting winding deformation.

The basic principle of FRA is change in winding geometry brings a corresponding change in resonant frequencies and parameters. The advancement of benefits of SFRA lies in identifying the changes in the fingerprint graph when compared with the reference with accuracy and precision. One approach, which has been adopted by many researchers, has been the use of a transformer model based on its geometric parameters [9, 11, 16].

The change in the winding configuration brings a change in its impedance and this changes the frequency response of the transformer. Before the advent of supercomputers, the frequency response of the power transformer was determined using punch card computing equipments, ac network analyzer methods, and matrix methods [1, 4, 5]. These three methods were used to determine frequency response of a model coil designed by K. K. Palueff [1]. The specialty of the model coil was it was already validated for experimental studies, its parameters could be modified as desired, and its range could match with that of the power transformer [1].

The benchmark considered here is helical test coil. An accurate and straightforward method was proposed to measure the frequency response characteristic of the transformer based on matrix approach [2]. Frequency-response analysis (FRA) is a commonly used diagnostic approach which looks for changes in the frequency response of a transformer. Each FRA test will yield a signature unique to the transformer's mechanical geometry from the perspective of the input and output measurement terminal positions. Changes in the frequency-response signature can be indicative of winding deformation. However, to date, there is relatively little understanding of how to interpret the underlying cause of the change directly from the frequency response [23].

A detailed evaluation of the relative merits of the two methods can be found in [21]. Briefly, the main advantage of the impulse response method over the swept frequency method is a shorter measurement time. The main advantages of the swept frequency method over the impulse response method are as follows are given in [9]:

- better signal to noise ratio
- equal, or nearly equal, accuracy and precision across the whole measurement range
- a wider range of frequencies are injected
- less measuring equipment is required

Any kind of fault that produces a significant change in the parameters like inductance and capacitance of the winding also brings a change in the frequency response and hence can be detected [11, 21]. To compare the graphs of the current response with the reference, statistical indicators like Correlation Coefficient (C.C.), Standard Deviation (S. D.), Absolute sum of logarithmic error (ASLE), etc. have been used [20, 24]. However, in [9], CC is considered as the most appropriate indicator as it is objective and transparent. Still, further research has led to the understanding that ASLE is better than CC in detecting faults mathematically [24]. Since the sensibility of SFRA has been already proved. There were problems if the reference is absent. In such situations, when the transformer lacks a reference, a sister unit was developed for substituting for the reference unit [9, 24], considering the tolerance limits for the numerical evaluation indicators.

Transfer function method to detect radial and axial deformation in a transformer was successfully carried in [16]. The author used two actual units of transformer to obtain the measurements for FRA study. A detailed model based on self and mutual inductance was proposed for the purpose of analyzing the deformations. It was found that radial deformation changed the frequency response over the whole range whereas axial displacement brought changes above 200 kHz. The location and extent of deformation was predicted using deformation coefficient method in [22].

1.4. Motivation

The demand for reliable supply of electrical energy has grown over few decades. The role played by power transformer towards power distribution without unwanted outages is of the highest importance. To prevent uneconomical outages, and maintain the reliability of power, routine diagnosis of the transformer becomes necessary to maximize its uptime. One of the

reasons of failure of the transformers is the deformations in the winding. The major cause of deformations in the winding is due to the effect of electromagnetic forces arising as an outcome of a short circuit fault. Various modeling techniques were employed to represent the equivalent circuit of the transformer winding. Modeling based on self and mutual inductance is found to give correct response as compared with the experimental results.

Various diagnostic techniques like reactance comparison method, dissolved gas analysis, furan analysis, low voltage impulse methods, etc. have been used for many decades. Still, the need of the time was a highly sensitive technique that could detect even minor deformation occurring in the winding structure. Sweep frequency analysis approach is a highly sensitive technique which has several advantages over other techniques.

1.5. Objectives

- Determination of changes in resonant frequencies observed due to parameter changes after winding deformation
- To use a sensitive approach like swept frequency analysis for diagnosis of transformer winding deformation or displacement
- Calculation of static forces through 2D modeling and simulation of transformer using FEM.
- To diagnose various types of deformations in the transformer winding to aid the designers and to increase the short circuit withstand capability.
- Calculation of parameters varied due to axial and radial deformations using finite element method.
- Determination of SFRA for the deformed cases and comparison of fingerprint graphs for the deformed cases with the reference fingerprint.
- Finding location and type of deformation after SFRA analysis.

1.6. Organization of Thesis

Chapter 1 consists of a brief overview of the topic, detection of deformation techniques, literature review, motivation, objectives and organization of thesis.

Chapter 2 describes about the short circuit forces and their effects, and modeling of transformer using finite element method (FEM) and calculation of axial force due to height shortening of one of the winding.

Chapter 3 consists of description of coil model, comparison of 10 section and 20 section coil model and application of sweep frequency response analysis (SFRA) to the healthy winding.

Chapter 4 consists of calculation of parameters using finite element method modeling for healthy and deformed winding.

Chapter 5 consists of SFRA analysis for axial and radial deformation applied to the coil model, and finding location and type of deformation from the observations.

Chapter 6 consists of summary of the work undertaken, future scope of the work, and references.

CHAPTER 2

PHYSICS OF WINDING DEFORMATION

2.1. Introduction
2.2. Short circuit forces
2.3. Modeling of a transformer using FEM
2.4. Conclusion

2.1. Introduction

The occurrence of short circuit faults is a major cause behind the winding deformation in the transformers. The short circuit current is 5 to 10 times higher than the normal current flowing in the windings. As the forces developed due to short circuit current is proportional to the square of the current, it will be very high. These forces cause the winding to deform radially or axially depending on the type of force acting on them. The computation of these forces is necessary to decide the short circuit withstand capability and to take necessary precautions to prevent the damage of transformers. Analytical approaches were found to be complicated when complex geometry was involved. Hence numerical modeling technique like finite element method approach (FEM) is found to give solution for computing forces, losses, and other required parameters, even for complex geometry. In this chapter, the short circuit forces and their effects along with an example of computing forces developed in transformer winding due to an axial asymmetry by using Finite element method (FEM).

2.2. SHORT CIRCUIT FORCES

Short circuit events generate large magnitude of current in the transformer winding. The interaction of the current and leakage flux density result in extreme electromagnetic forces to act on the winding. The basic equation for the calculation of electromagnetic forces is

$$\mathbf{F}=L\,\mathbf{I}\times\mathbf{B} \tag{1}$$

Where **B** is leakage flux density vector, **I** is current vector and L is winding length.

There are basically two categories of short circuit forces involved in the deformation action on the transformer windings, which are axial force defined by expression in (2) and radial force defined by expression given in (3). In Fig. 2.1 (b), the resolution of forces and leakage flux density in radial and axial direction is shown. The leakage flux density can be resolved into two components, one in the radial direction, ($\boldsymbol{B_x}$) and the other in the axial direction, ($\boldsymbol{B_y}$).

The action of radial leakage flux density with the current density ***(J)*** results in axial force ($\boldsymbol{F_y}$).

$$\boldsymbol{F_y = \iint (J \times B_x)\, dx\, dy} \tag{2}$$

Similarly, the interaction of axial leakage flux density with the current density results in radial force ($\boldsymbol{F_x}$).

$$\boldsymbol{F_x = \iint (J \times B_y)\, dx\, dy} \tag{3}$$

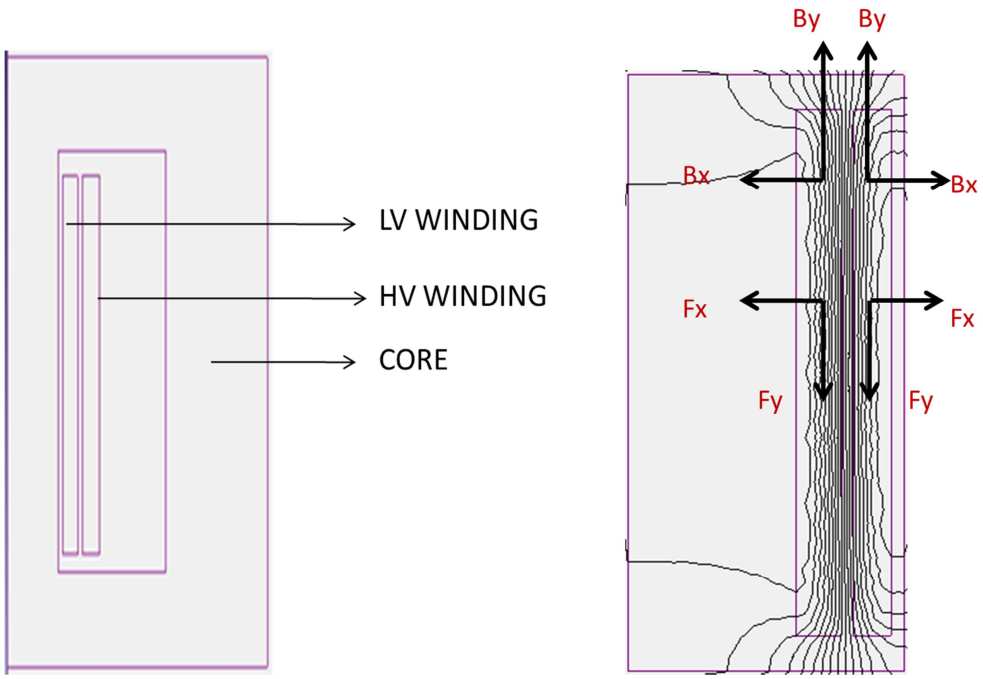

Fig. 2.1(a): Cross sectional view of the core and the windings of a 66/11 KV,40 MVA transformer. Fig. 2.1(b) Flux and forces distribution of 40MVA transformer simulated using FEM (finite element method)

The direction of forces is apparent from Fleming's left hand rule. Forces experienced by a winding are proportional to the square of the short circuit current and are unidirectional and pulsating in nature. It is required to resolve the short circuit forces into radial and axial forces to study their influence on the winding structure due to various failure modes [11].

2.2.1. Radial forces

The forces generated by the action of axial leakage field and perpendicular to the direction winding height are called the radial forces. The axial field is maximum at the middle part, in the air gap between the two windings. Hence the radial force will be maximum at that portion too. The forces acting on the inner winding produces a compressive stress and that acting on the outer winding produces a tensile stress. Let us consider an outer winding, which is subjected to hoop stresses. The value of the leakage field increases from zero at the outside diameter to a maximum at the inside diameter (at the gap between the two windings). The peak value of flux density in the gap is given in (4).

$$B_{gp} = \frac{\sqrt{2}\, NI\mu_o}{H_w} \tag{4}$$

Where NI is the R.M.S value of winding ampere-turns and H_w is winding height in meters. The whole winding is in the average value of flux density of half the gap value. The total radial force acting on the winding having a mean diameter of D_m (in meters) can be calculated as [11]:

$$F_x = \left[\frac{1}{2}\,\frac{\sqrt{2}\, NI\mu_o}{H_w}\right] \times \sqrt{2}\, NI \times \pi D_m \tag{5}$$

For the outer winding, the conductors close to gap (at the inside diameter) experience higher forces as compared to those near the outside diameter (force reduces linearly from a maximum value at the gap to zero at the outside diameter).

The effects of radial forces are the tensile stress on the winding resulting in forced buckling and free buckling as shown in Fig. 2.2(a) and (b) respectively.

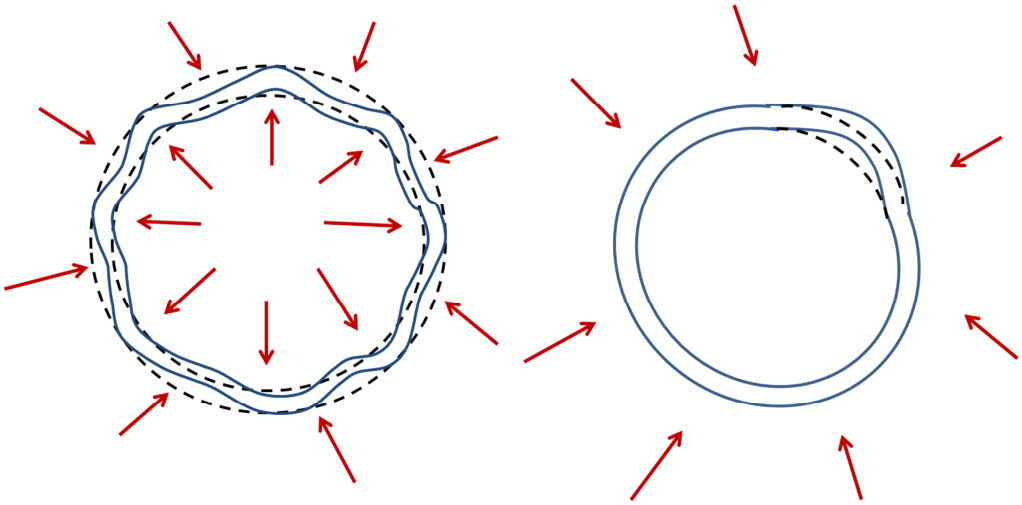

Fig. 2.2(a): Forced Buckling

Fig. 2.2(b): Free Buckling

The failure modes for radial forces include

- Forced mode Buckling
- Free mode buckling
- Stretching of outer windings and spiraling of end turns in helical windings

2.2.2. Axial forces

The forces generated by the action of radial leakage field and acts in a direction parallel to the winding height is called as axial forces. The influence of axial forces will be maximum at the winding ends causing maximum bending of the conductors. The forces produce compressive stress on the winding conductors which acts towards the center of the winding. The axial forces are maximum at the ends of the winding as the radial leakage field between the two windings is maximum at the ends. While the axial forces will be minimum at the center as the axial leakage field is maximum between the air gap of the two windings.

For an asymmetry factor of 1.8, the total axial compressive force acting on the inner and outer windings taken together is given by the following expression:

$$F_y = \frac{50.8 \times \mathrm{S}}{Z_{pu} \times H_w \times \mathrm{f}} \tag{6}$$

Where S is rated power per limb in KVA, H_w is winding height in meters, Z_{pu} is per-unit impedance, and f is frequency in Hz. The inner winding being closer to the limb, by virtue of higher radial flux, experiences higher compressive force as compared to the outer winding. In the absence of detailed analysis, it can be assumed that 25 to 33% of force is taken by the outer winding, and the remaining 75% to 67% is taken by the inner winding.

The reasons for a higher value of radial field and consequent axial forces are: mismatch of ampere-turn distribution between LV and HV windings, tapping in the winding, unaccounted shrinkage of insulation during drying and impregnation processes, etc.[11]

The failure modes for axial forces include:

- Conductor tilting
- Conductor axial bending between spacers
- Displacement of the complete winding
- Axial overlap of conductors

Fig. 2.3(a) : 100 MVA power transformer without any deformation

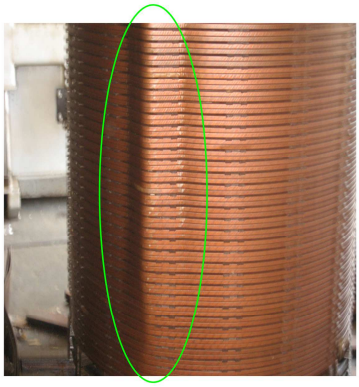

Fig. 2.3(b) : Free mode buckling

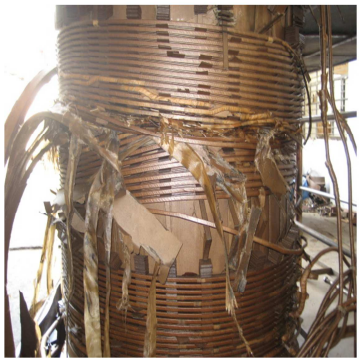

Fig. 2.3 (c): Axial deformation

2.3. Finite Element Method (FEM) modeling of a transformer

In FEM approach, the problem geometry is divided into small elements of triangular or tetrahedral shape within which the flux density is assumed constant so that the magnetic vector potential varies linearly within each element. This numerical modeling technique is a highly recommended method for analyzing any heterogeneous complicated geometry.

Table 2.1: Design specifications [18]

Winding	Inner radius mm	Outer radius mm	Height mm	Turns	Rated Current(A)
LV winding	306.5	388	1136	200	2100
HV winding	413	510.5	1136	1200	350

A transformer of 40 MVA rating is designed with specifications as given in Table 2.1 and Fig. 2.4 shows the coordinates of the required design. Using these data in Table I and design coordinates of Fig., model is designed in FEM based software MAGNET as shown in Fig 2.5. The material used for core is silicon steel, copper for the transformer windings and the whole model is enclosed in an airbox which acts as boundary. At normal operating conditions and identical winding symmetry, rated current will flow through the primary and secondary windings. However, if the any asymmetry arises due to shortening of height of one of the windings, the forces developed in such case is very high resulting in unequal end thrust at the

ends of the windings. The reason behind this is large magnitude of current in the winding resulting in large forces top act on them.

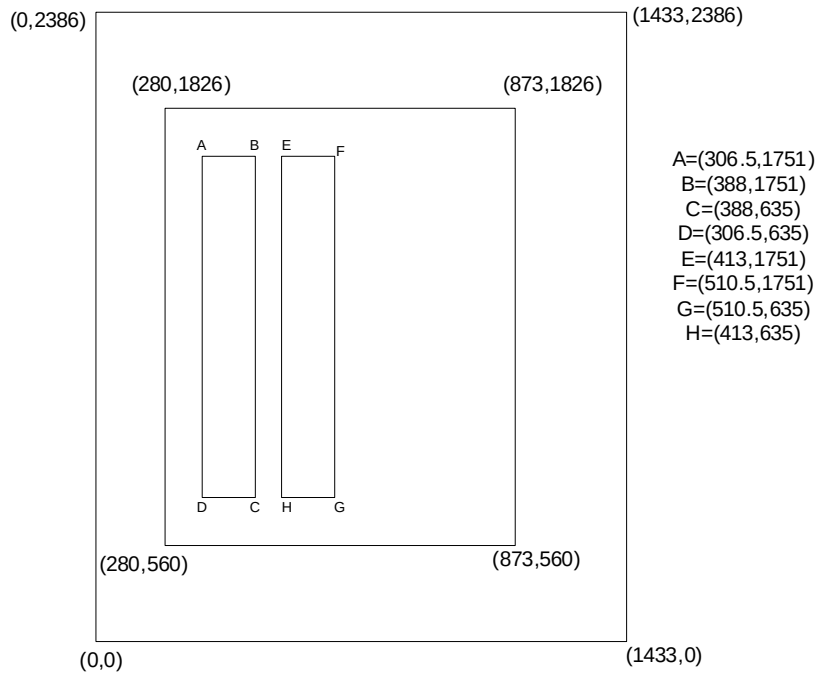

Fig. 2.4: geometry coordinates of transformer

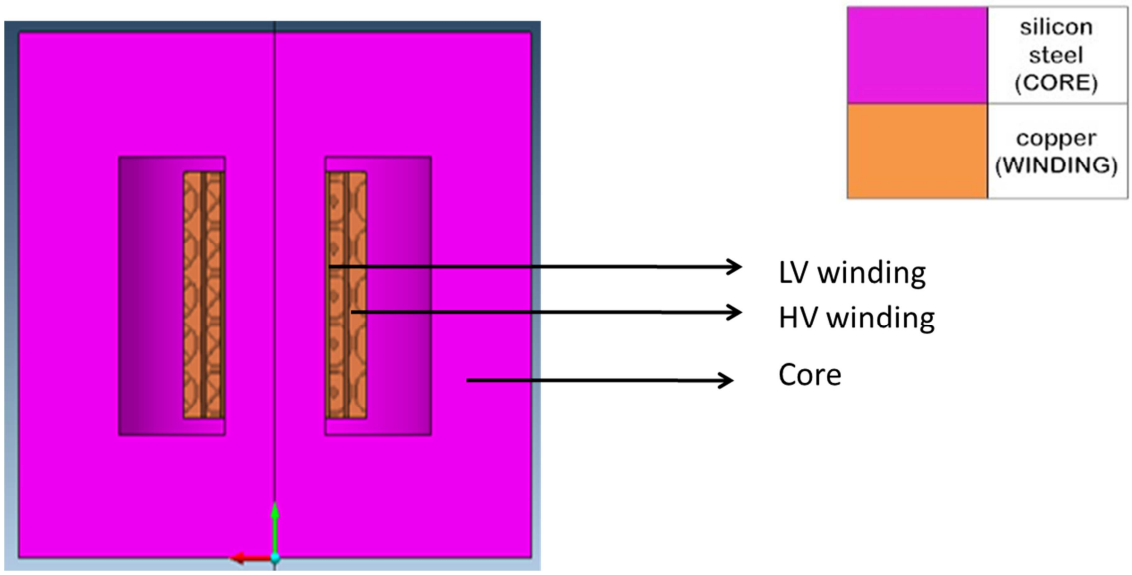

Fig. 2.5 Cross-sectional view of the FEM modeled transformer

Rated current flows through the primary and secondary windings of the transformer during normal operating conditions. The current in the lv and hv windings are calculated as given in (6) and (7).

$$I_{hv} = \frac{P \times 10^3}{\sqrt{3} \times V_l} = \frac{40 \times 10^3}{\sqrt{3} \times 66} = 349.90\ A \tag{7}$$

$$I_{lv} = \frac{P \times 10^3}{\sqrt{3} \times V_l'} = \frac{40 \times 10^3}{\sqrt{3} \times 11} = 2099.45\ A \tag{8}$$

Where, P is MVA rating of the transformer,

$I_{hv} and\ I_{lv}$ are current in the hv or primary winding, and lv or secondary winding respectively,

$V_l and\ V_l'$ is the line voltage across primary winding and secondary winding respectively.

And $\frac{N_1}{N_2} = \frac{V_l}{V_l'} = \frac{I_{lv}}{I_{hv}} = 6$

After simulation using FEM, the flux pattern and shaded plot of magnetic flux density can be observed as shown in Fig. 2.6 (a) and (b). Maximum flux density exists between the hv and lv winding which is 0.468 T. The main reason behind the low value of flux density is the area of the 2D transformer model which is very less as compared to the actual transformer.

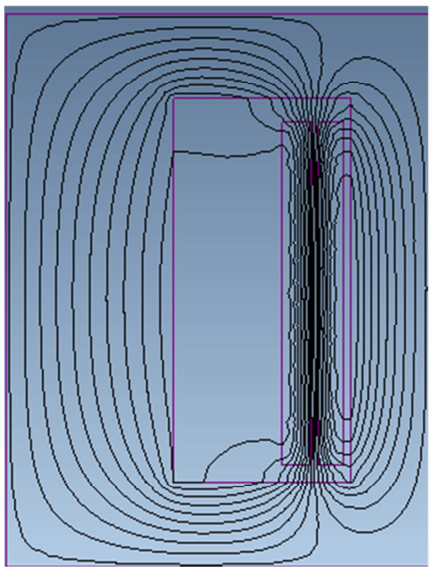

Fig. 2.6 (a) Flux pattern

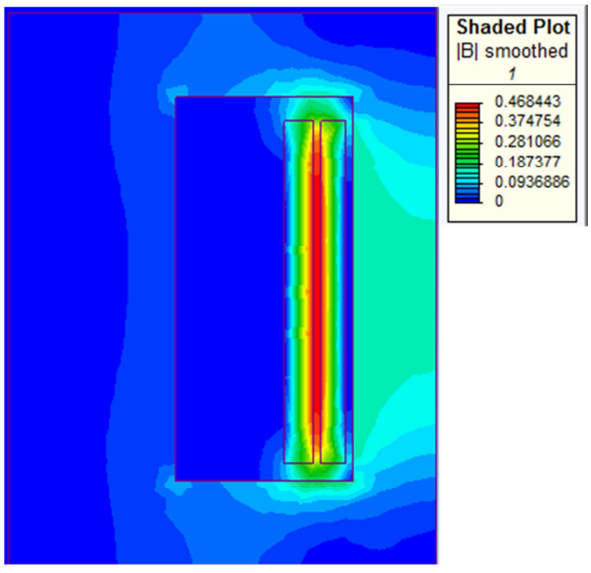

Fig. 2.6 (b) Shaded plot of magnetic flux density

2.3.1. An example of study of axial deformation through FEM modeling

Any kind of asymmetry between the height of the two windings, mismatch of ampere turns, which may result due to shortening of the height of one of the windings, is capable of creating large axial force. Now, let the height of the HV winding be reduced to 1% of the original height. The forces obtained are much greater than that in normal case as the short circuit current results to flow in the windings which are assumed to be 8 times than that of the normal rated current [11]. To calculate and compare the forces developed due to the described situation is analyzed using finite element method (FEM).

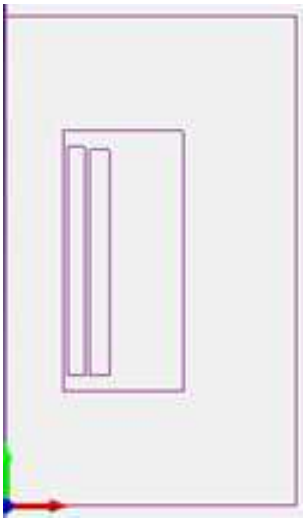

Figure 2.7: shortened height (1%) of the HV winding

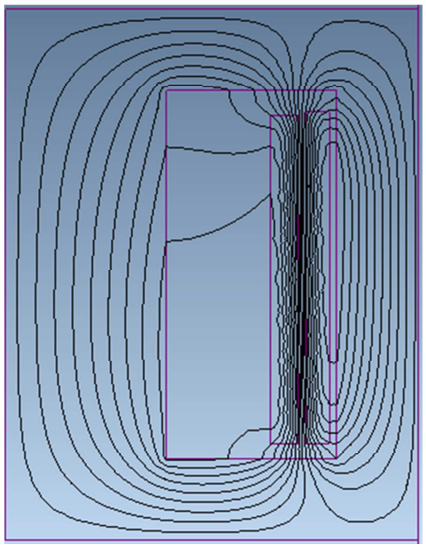

Fig. 2.8 (a) Flux pattern

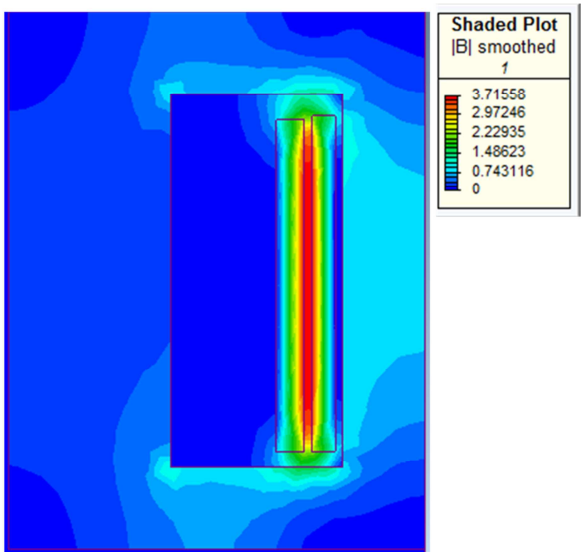

Fig. 2.8 (b) Shaded plot of magnetic flux density

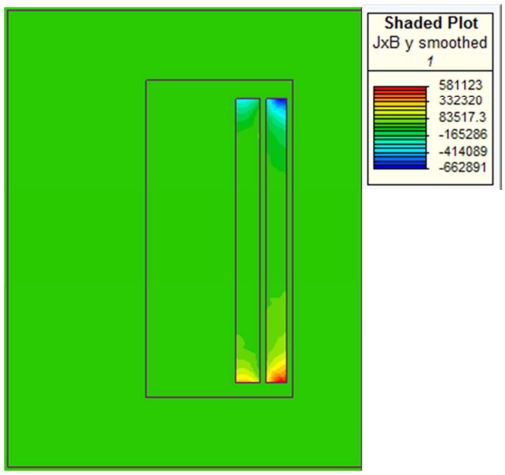

Fig. 2.9 (a) Axial force distribution at normal condition

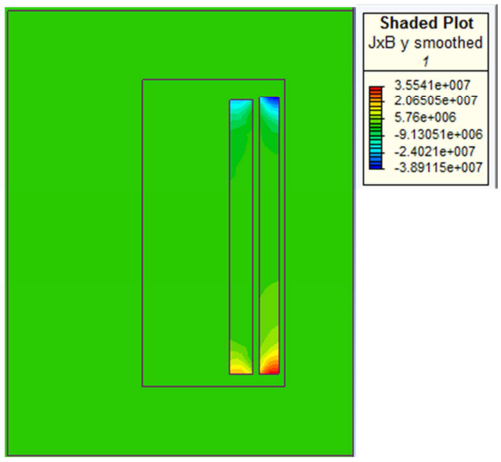

Fig. 2.9 (b) Axial force distribution due to asymmetry

Table 2.2: Comparison of forces

Element	Average Force without deformation(N)	Average Force with deformation(N)
LV winding	7.72370192	7.44×10^{6}N
HV winding	0.00014233	5.25×10^{6}N

The table clearly shows the variation of forces with change in height of one the windings. when both the windings were of same height and the electrical centers were coinciding the forces were almost nil. However when the height of one of the winding, here the HV winding was shortened, the axial force magnitude increased manifold. The end thrust will be more at the ends of the windings. Such kind of deformation will give rise to compression or expansion of the winding height.

2.4. Conclusion

The short circuit forces are the main cause of winding deformation and displacement arising in power transformers. Using numerical modeling approach like FEM, the study of winding deformation through computation of forces and other requirements can be met. Further, the method is applicable for complex geometrical structures like transformers, which is advantageous over other analytical techniques.

CHAPTER 3

HIGH FREQUENCY MODELING OF POWER TRANSFORMER

3.1. Introduction
3.2. Winding under test
3.3. Frequency Response characteristics of 10 section and 20 section models
3.4. Comparison of 10 section and 20 section models
3.5. Conclusion

3.1. INTRODUCTION

Power transformers are essential component in a power industry and its failure can cause serious problems. The transformer manufacturers strive towards maintaining maximum efficiency and reliability. The winding parameters, short circuit reactance, and short circuit forces need accurate evaluation to avoid mechanical damage due to short circuit events occurrence. The analytical approaches used for the calculation of forces and parameters are not accurate and can solve for simple/homogenous transformer geometries. However for complex transformer geometries, numerical modeling approach such as finite element method (FEM) is found to be providing accurate and precise solutions. The main advantage of FEM is that any complex geometry can be analyzed as its formulation depends only on the type of problem rather than its geometry [11].

With the development in digital world, it has become easier to model the complicated equipments for the power industry. The lumped model representation was found to give good results for the study of transient voltage response and effect of switching surges in the structures. The knowledge of frequency response of transformer windings can be easily determined with the help of the lumped network. The location of zeros and poles of the impedance function of any circuit in the complex frequency plane is required for the analysis of steady-state and transient behavior of the circuit.

Before the advent of high speed computers, natural frequencies of a transformer winding were determined by punch card computing equipments and a-c network analyzer methods. In 1977, a mathematical approach using matrix methods was applied for the calculation of natural frequencies. The advancement in digital technology has led to still simpler ways of finding the natural frequencies. In this paper, computational approach using MATLAB is applied for the calculation of resonant and anti-resonant frequencies. A single layer helical winding having similar lumped parameter network as a transformer winding as given in [2] is chosen for the purpose of obtaining the frequency response. Further, the coil can be represented as finite number of sections.

The choice of representing the coil as finite number of sections depends on the number and accuracy of required natural frequencies. The coil is represented as 10 section and 20 section models. A 10 section model is a commonly accepted model for the study of frequency response of

a transformer winding [2], [11]. However, a 20 section model can be beneficial in certain areas where 10 section model does not meet the requirements. In this paper, a comparison is carried, of 10 section and 20 section models, by a discussion on the benefits and drawbacks of using either of them

3.2. WINDING UNDER TEST

A single layer helical air core coil is chosen for the study of frequency response characteristics in a transformer winding [1], [2]. The reason for choosing the coil is that the parameters could be varied within wide limits at will and the range could match with that of power transformers [1]. The coil described was designed by K. K. Palueff [1]. The coil consists of a uniform helical winding with 1794 turns, 0.0226 inch of circular copper wire, 0.00205 inch enamel coating, wound on a 23 inches air core, 48 inches in length. It is surrounded by inner shield of diameter 22.69 inches and outer shield of 25 inches diameter [2]. The inner and outer shield represents the transformer core and tank respectively. The helical test coil can be represented by an equivalent circuit as shown in Fig. 3.1 and consists of series resistance (R_s), series capacitance (C_s), ground resistance (R_g) and ground capacitance (C_g), self-inductance (L_{ii}) and mutual inductance (M_{i-j}).

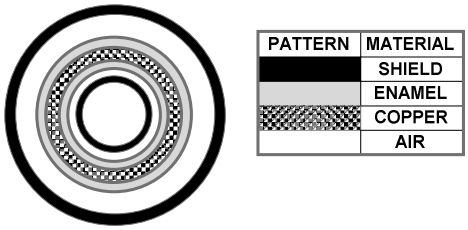

Fig. 3.1 Cross-sectional view of the helical coil

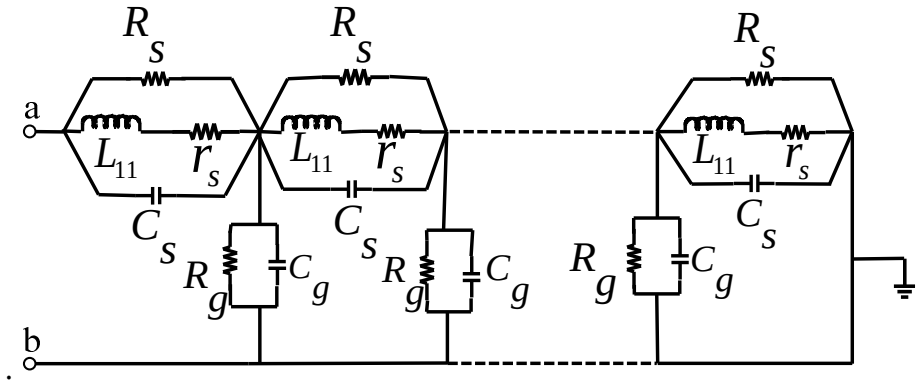

Fig. 3.2 Equivalent circuit of helical test coil

At high frequency, the equivalent circuit of a transformer is similar to shown in Fig. 1. At low frequency, the series and ground capacitance, self and mutual inductances were neglected. However, at higher frequencies, these parameters have a significant effect on the behavior of the circuit and hence considered.

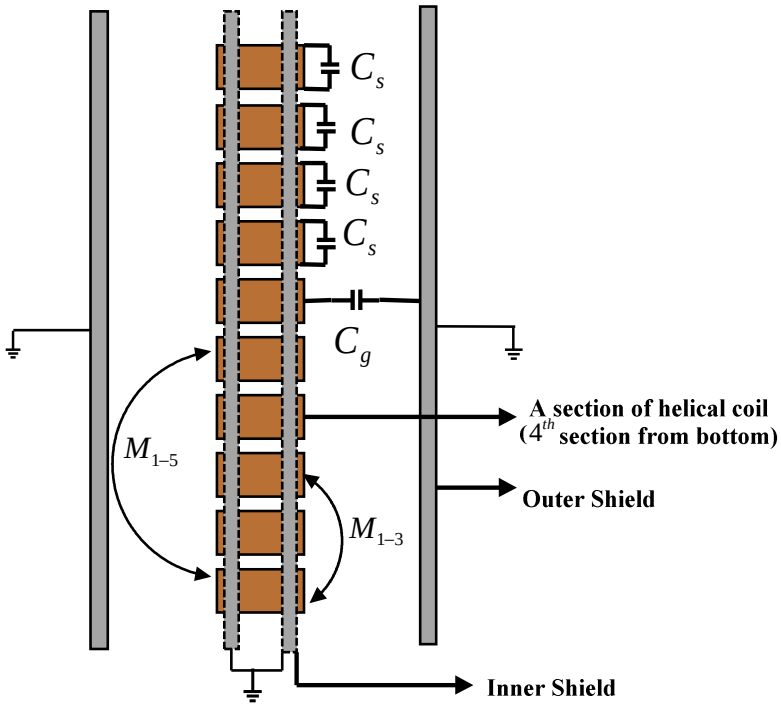

Fig. 3.3 Physical representation of parameters.

The physical representation of parameters is shown in Fig. 3.3 which also illustrates the physical meaning of the parameters and is not as per the specified dimensions. The series capacitance is the equivalent capacitance between the turns of the section [1, 11]. The ground capacitance exists between the coil and grounded shields. For a healthy winding, the ground capacitance remains identical for all the sections. The change in geometry of winding also changes the parameters.

3.2.1. Frequency Response Characteristics Of 10 Section And 20 Section Models

Usually, natural frequencies of a multi section network is found by applying a sustained constant voltage varied over a sufficiently wide range in frequency and to measure the impedance and current at each frequency. The frequency response characteristics of the coil are determined.

The lower end of the coil is solidly grounded. A sinusoidal voltage signal of constant magnitude of 1 volt is applied at its upper end, at a range of frequencies from 50 Hz to 100 KHz at an interval of 50 Hz. Such a method of sweeping a sinusoidal signal of constant amplitude at the input terminals of a specimen winding is termed as sweep frequency response analysis (SFRA).

The resistance and capacitance values are referred from literature [2]. The self and mutual inductance are derived from the tables and formulas provided in [12]. Parameter values for all the sections are given in Appendix I.

Fig. 3.4, 3.5 and 3.6 show the variation of input current, resistance, and reactance respectively, with frequency for both 10 section and 20 section model. The points of maxima on the curve in Fig. 3.4 are the points of resonant conditions in the circuit, with input current maximum, and minimum impedance (resistive) as shown in Fig. 3.5. At resonance, the inductive reactance and capacitive reactance cancel each other as shown in Fig. 3.6. The points of minima shown in Fig. 3.4, correspond to anti-resonant frequencies, with the input current minimum and resistance maximum. The points of series and parallel resonance are then taken to correspond to the maximum and minimum points of the curve.

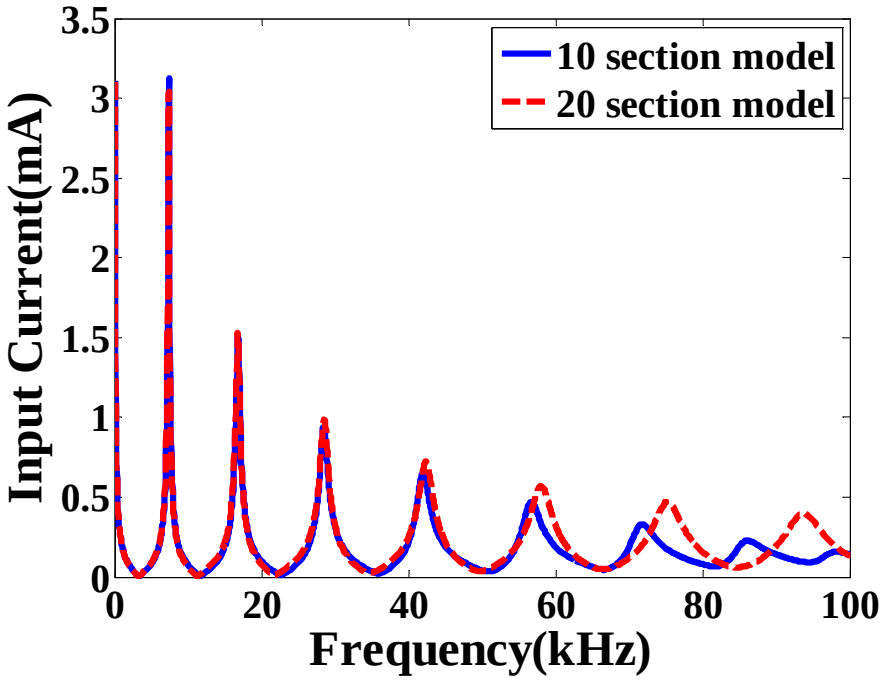

Fig. 3.4 Input current response

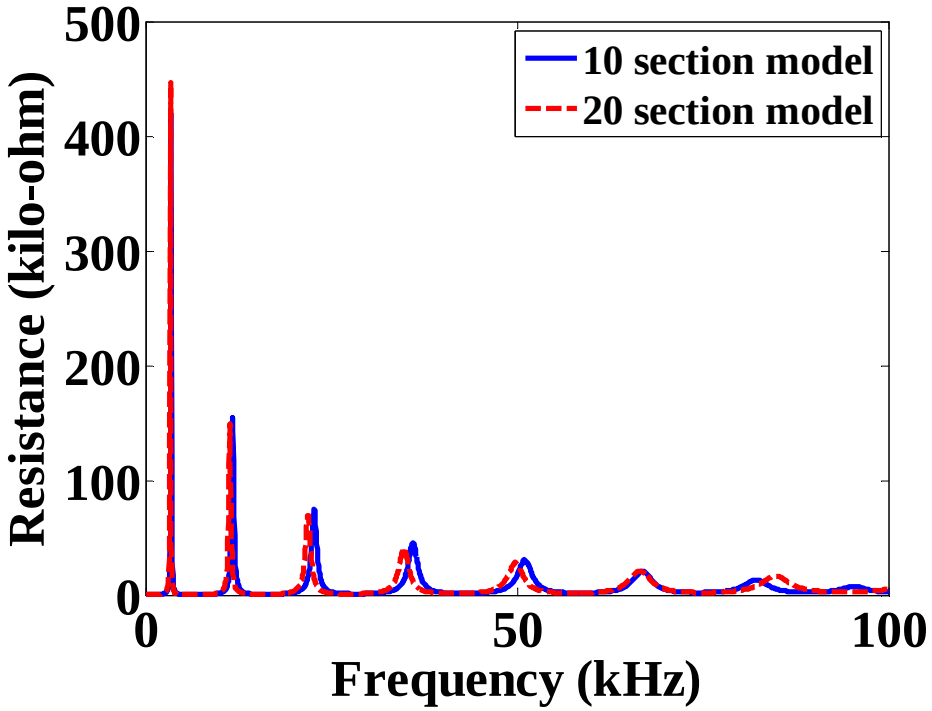

Fig. 3.5 Resistive Plot

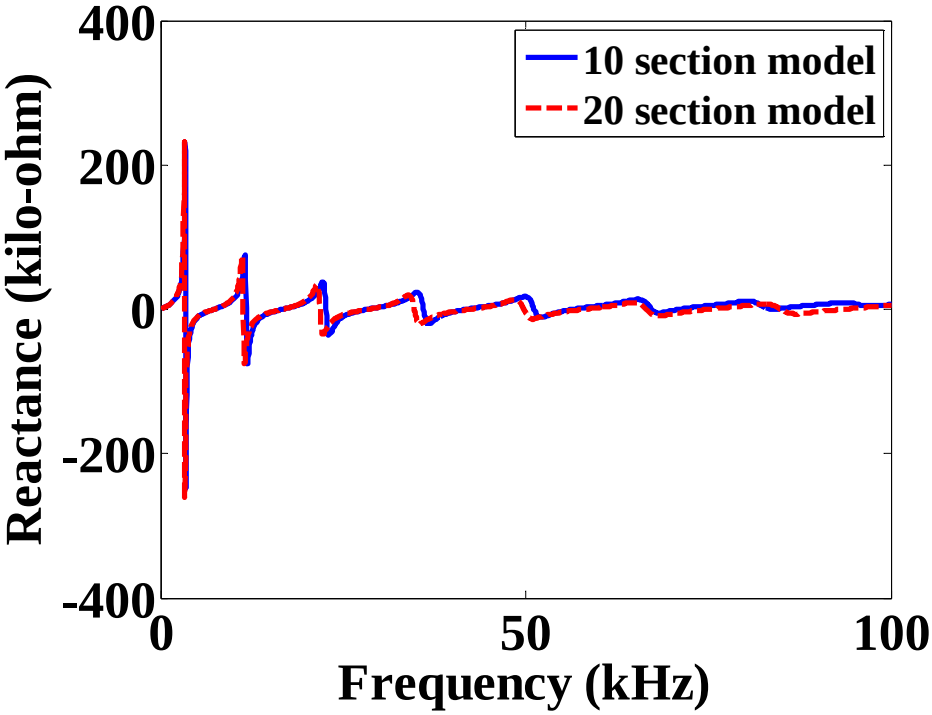

Fig. 3.6 Reactive Plot

3.3. Comparison of 10 and 20 section Models

Comparison of models is carried out on the basis of:

1. Accuracy of computation
2. Computational time and memory requirement
3. Complexity in transfer function computation

The main objective behind the comparison is to derive an optimal model for analysis of deformation in the transformer winding.

3.3.1. Accuracy of computation

Measured resonant and anti-resonant frequencies are given in [1], [2]. The calculated frequencies for both 10 and 20 section models are compared with the measured values as shown in Fig. 7.

$$acc_n = \frac{(Measured\ value - Computed\ value)}{Measured\ value} \times 100 \quad (1)$$

As the calculated and measured values have a very small difference, they are not so much distinct in Fig. 7. To properly observe the difference tabular representation is required as shown in Table 3.1. At lower harmonic order, the calculated and measured values are quite agreeable. The calculated frequencies for 10 section model are found to deviate more from the measured frequencies from the 5th order. However, the 20 section model is found to closely agree with the measured values till 7th order. The accuracy limit for 20 section model is thus higher than for 10 section model.

3.3.2. CPU time computation and memory requirement

The CPU time (system used was $Core^{TM}$ 2 Duo processor, 2.20 GHz, 3 GB RAM) needed to determine the frequency response for the circuit given in Fig. 1, with 10 section and 20 section model is 2.26 seconds and 10.49 seconds respectively. The comparison of CPU time shows that the execution of MATLAB code for 10 sections is faster than for 20 sections. As the nodal matrices of inductance and conductance are of dimension n × n, where n is the number of sections. The nodal matrices for 20 section model will contain 20×20 = 400 elements while the same for 10 section model will contain 100 elements. Hence, the memory requirement for individual nodal matrices of 20 section model will be 4 times that for 10 section model.

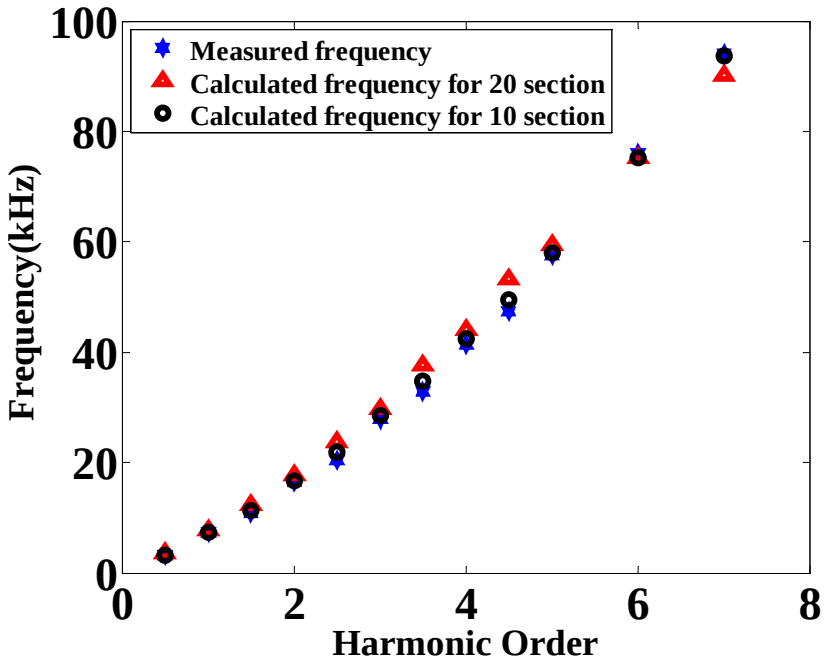

Fig. 3.7 Comparison on the basis of accuracy of measurement

TABLE 3.1 Comparison of accuracy in measurement

H	m	f_{20}	f_{10}	acc_{20}	acc_{10}
0.5	3.15	3.30	3.43	4.76	8.89
1	7.35	7.40	7.40	0.68	0.68
1.5	10.80	11.30	11.75	4.63	8.70
2	16.50	16.80	16.80	1.82	1.82
2.5	20.50	21.80	22.70	6.34	10.73
3	28.00	28.55	28.50	1.96	1.78
3.5	32.90	34.80	35.80	5.77	8.81
4	41.40	42.35	42.00	2.29	1.44
4.5	47.50	49.55	51.00	4.31	7.37
5	57.50	58.05	56.70	0.96	1.39
6	76.00	75.25	71.80	0.99	5.53
7	94.00	93.70	86.20	0.32	8.29

H is Harmonic Order, decimal number specifies anti-resonance and integral order specifies resonance, **m** is Measured Frequency (kHz), f_{20} and f_{10} are calculated frequency (kHz) for 20 sections and 10 sections respectively, acc_{20} and acc_{10} are percentage of deviation from measured values or inaccuracy, for 20 sections and 10 sections, respectively.

3.3.3. Complexity in matrix computation without diagonalization

The most general form of the state equations of a linear, time- invariant network is as follows:

$$\dot{x} = [A]x + [B]u \tag{3}$$

$$y = [C]x + [D]u \tag{4}$$

Where,

x is the column vector of the state variables;

$\dot{x}$ is the time derivatives of the state variable;

u is the excitation or input vector;

y is response or output vector;

(A, B, C, D) are matrices of constant coefficients.

$$T.F. = C[sI - A]^{-1}B + D \tag{5}$$

The problem with the large number of sections is seen, when the computation is done without diagonalization of the system and nodal matrices. The computation problem can however be solved by diagonalization of the inverse matrix.

3.4. APPLICATION OF SFRA ON THE HEALTHY WINDING

SFRA is a powerful and highly sensitive diagnostic technique. Here, a 10 section healthy coil is considered for the application of SFRA. A constant input voltage of 1 volt is swept across the winding at a range from 50 Hz to 100 kHz. The impedance and input current as a function of frequency are observed from the simulation. The SFRA fingerprint graphs are taken as reference for further analysis and comparison after modeling axial and radial deformations.

The input current and impedance waveforms have continuous decreasing amplitude with increasing harmonic order. In the Fig. 3.8, maximum points of the graph correspond to resonant frequencies while the minimum points correspond to anti-resonant frequencies. Also from Fig. 3.9, it is evident that at points of resonance, the equivalent circuit is resistive in nature, with capacitive and inductive reactance opposing each other to cancel each other's effect. Also it is observed that at frequency lower than a resonant frequency point, the capacitive effect is dominant, while at a frequency higher than the resonant point, the inductive effect is dominant. At points of resonance, the current is maximum and impedance is minimum while at points of anti-resonance, the current is minimum and impedance is maximum.

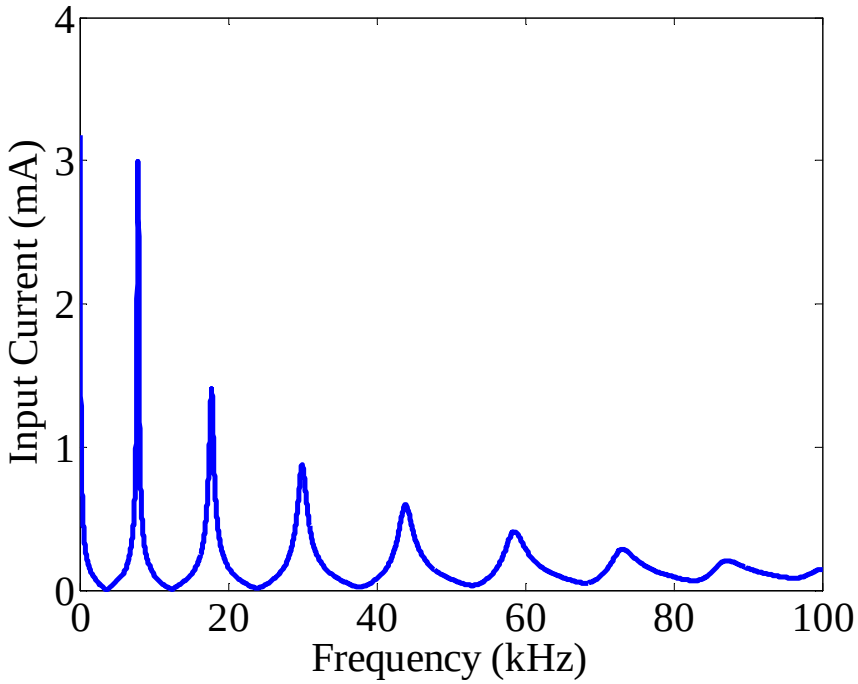

Fig. 3.8 Input current response for healthy winding

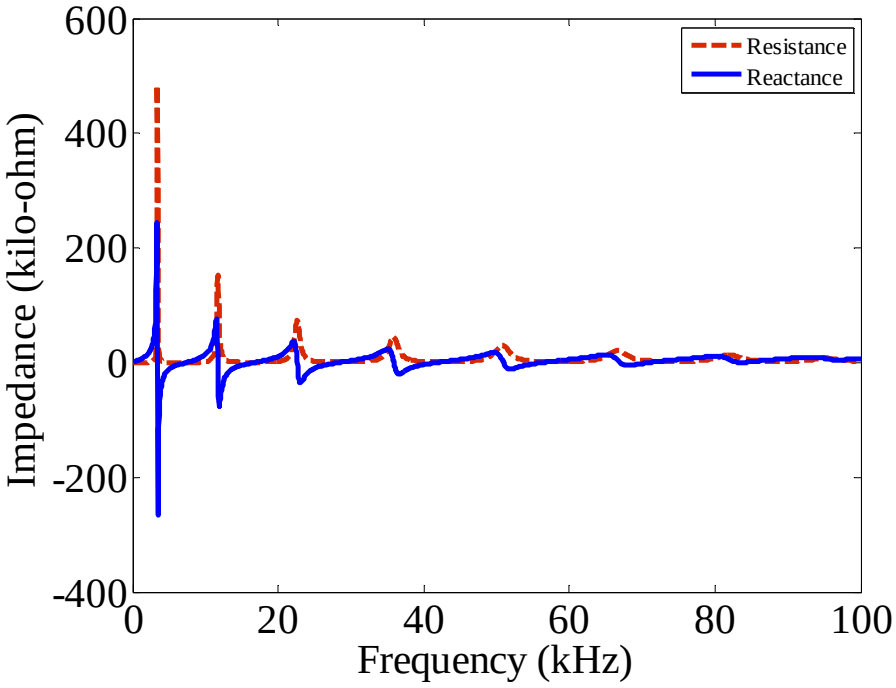

Fig. 3.9 Impedance plot for healthy winding

3.5. CONCLUSION

The benchmark winding exhibiting a similar high frequency behavior whose parameters match with an actual transformer is chosen for the analysis. The winding can be modeled as 10 section and 20 section models. It is found by comparison of both models that optimum model for the deformation analysis is a 10 section model as it involves less complexity although it is somewhat less accurate than 20 section model. SFRA is applied to obtain the impedance and input current plots for healthy 10 section coil model.

CHAPTER 4

PARAMETER CALCULATIONS

4.1. Introduction
4.2. Calculation of parameters for healthy coil model
4.3. Calculation of parameters for radially deformed coil
4.4. Calculation of parameters for axially deformed coil
4.5. Conclusion

4.1 INTRODUCTION

Any change in the physical configuration of a transformer winding also brings a change in the values of inductance and capacitance of its lumped parameter model. The optimum model chosen for the purpose of modeling deformations is the 10 section helical coil. In this chapter, parameters like series and ground capacitance, self and mutual capacitance are calculated using FEM based softwares for healthy, radially and axially deformed models. Here, the deformation is carried at five consecutive last sections in radial and axial directions. The main purpose of computing these parameter values is to carry out a sweep frequency response analysis for the deformed models and compare the obtained plots with the reference plot.

4.2. MODELING OF HELICAL COIL USING FEM

The main purpose of modeling of helical coil under test is to evaluate the parameters for the healthy condition and apply SFRA to obtain the fingerprint which will be the reference for the analysis of deformation in the winding.

The parameters to be calculated are those affected or changed after deformation such as series capacitance, ground capacitance, and self and mutual inductance.

For the purpose of calculating series and ground capacitance, FEM based ELECNET software is used. While for calculating the inductances the FEM based MAGNET software is used.

4.2.1. Self and mutual inductance calculations

For finding the value for self and mutual inductances, the single layer helical coil is modeled as shown in Fig. and the bottom coil(1^{st} coil) is excited with 1 Ampere and the other coils are unexcited. After solving the model in 2D as shown in Fig. 4.1, the results obtained includes Flux linkage for all the coils. The flux linkage for coil 1 gives its self-inductance value while the other coils experience mutual flux linkage and the mutual inductances as shown in Table 4.1 can be obtained.

Table 4.1 Self and mutual inductance in mH for healthy winding

L_{11}	M_{1-2}	M_{1-3}	M_{1-4}	M_{1-5}	M_{1-6}	M_{1-7}	M_{1-8}	M_{1-9}	M_{1-10}
28.81	12.87	5.731	3.012	1.7126	1.0302	0.649	0.4223	0.2848	0.19427

Fig. 4.1(a) FEM model of helical test coil for calculation of inductance

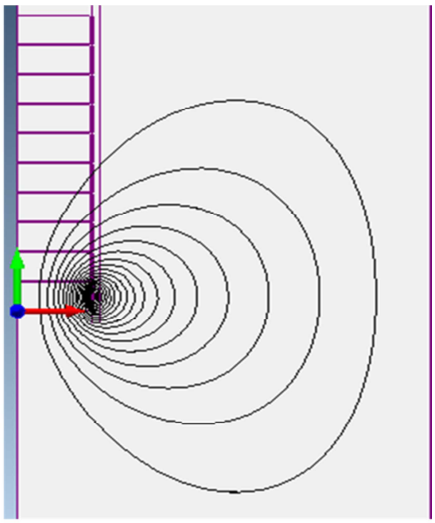

Fig. 4.1(b) Flux pattern with bottom coil energized

4.2.2. Series capacitance calculations

The series capacitance exists between individual adjacent turns of the helical coil as shown in Fig. 4.2. The equivalent series capacitance between the turns of a section will result in the series capacitance of a section.

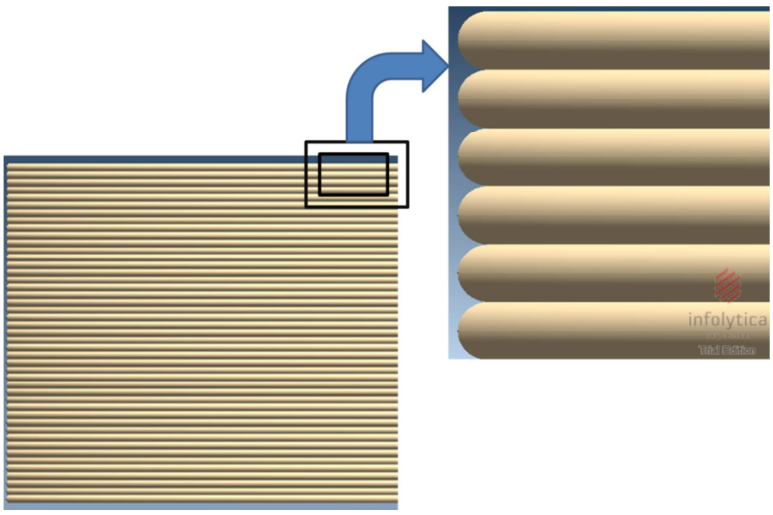

Fig. 4.2 Model designed for calculation of series capacitance

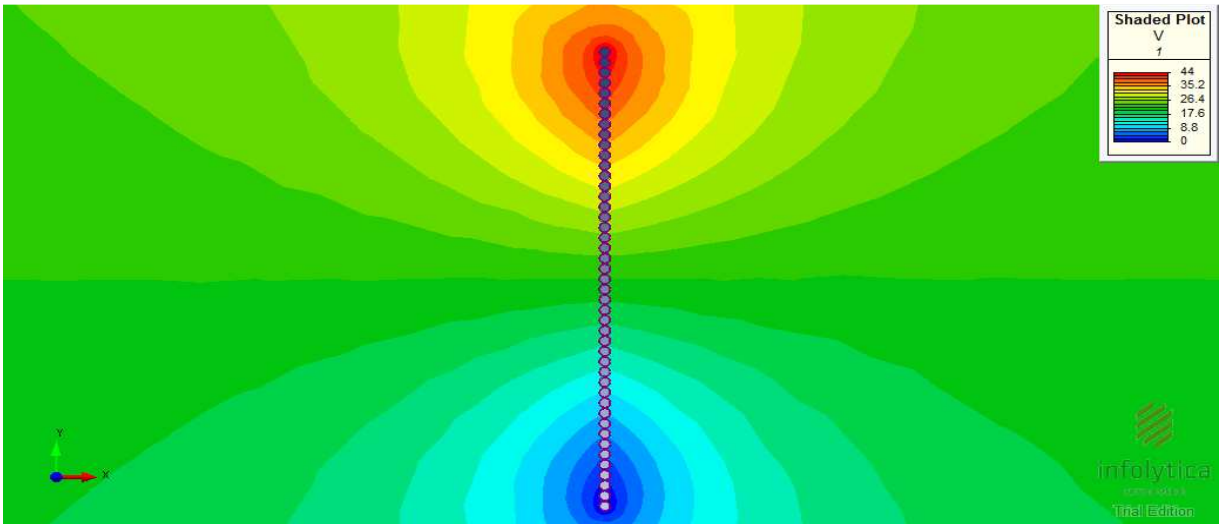

Fig. 4.3 Shaded plot of electric potential function

Stored Energy from simulation results of FEM, $W_{el} = \frac{1}{2} C_1 V^2 = 1.63 \times 10^{-8} J$

$$C_1 = 1.68 \times 10^{-12} F$$

Here, series capacitance is calculated for 45 turns of a section, which is $^1/_4\, th$ of a section. Hence equivalent series capacitance for the whole section is given in (n).

$$C_s = \frac{C_1}{4} = \frac{1.68 \times 10^{-12}}{4} = 4.2 \times 10^{-12} F \quad \text{(n)}$$

4.2.3. Ground capacitance calculations

For ground capacitance calculations, the electrodes are excited with 1 volt and the capacitance for different sections can be found. The model designed is similar to that for inductance calculations; only it is developed in ELECNET.

Table 4.2: Ground capacitance in nF, for healthy winding

C_{g1}	C_{g2}	C_{g3}	C_{g4}	C_{g5}	C_{g6}	C_{g7}	C_{g8}	C_{g9}	C_{g10}
0.7918	0.7769	0.7788	0.7628	0.7592	0.7619	0.767	0.767	0.7717	0.7893

C_{gi} is the capacitance to ground for *i*th section, where i=1,2,3,…..,10

4.3. RADIAL DEFORMATION

The helical coil is deformed radially by 7% of the coil radius which comes to be 0.8 inch. This deformation is carried for five sections individually. The model of the radially deformed coil is shown in Fig. 4.4 developed using FEM. The parameters affected are ground capacitance, self and mutual inductance.

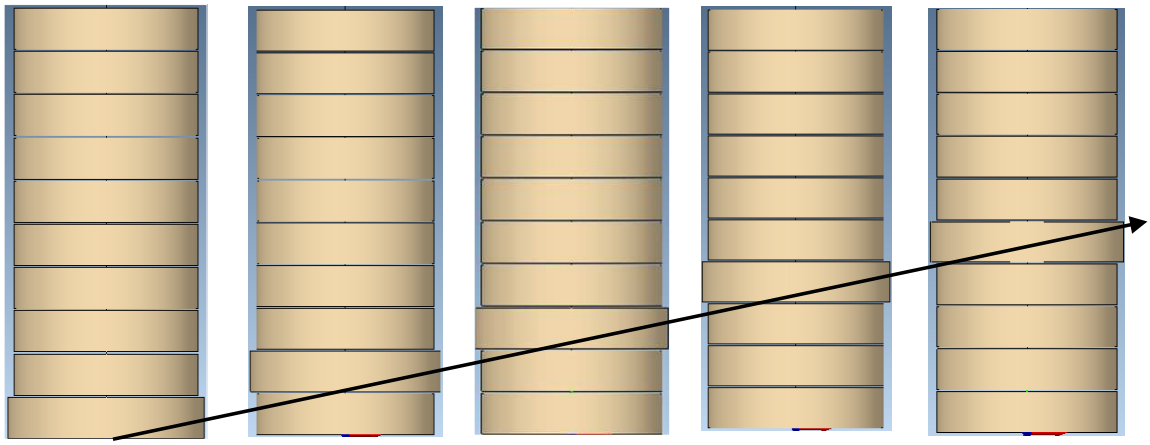

Fig. 4.4 Model designed using FEM to analyze radial deformations

4.3.1. First section radially deformed

Capacitance to ground for deformed section, C_{g1} = 6.9×10^{-10}F. The inductance values as computed using FEM is given in Table 4.3.

Table 4.3 Self and mutual inductance in mH

L_{11}	M_{1-2}	M_{1-3}	M_{1-4}	M_{1-5}	M_{1-6}	M_{1-7}	M_{1-8}	M_{1-9}	M_{1-10}
31.712	13.337	6.152	3.284	1.887	1.444	0.724	0.473	0.320	0.219

4.3.2. Second section deformed radially

The affected parameters, Capacitance to ground (C_{g2}) = 7.64 ×10^{-10}F**.** The inductance values as computed using FEM is given in Table 4.4.

Table 4.4 Self and mutual inductance in mH

L_{22}	M_{2-1}	M_{2-3}	M_{2-4}	M_{2-5}	M_{2-6}	M_{2-7}	M_{2-8}	M_{2-9}	M_{2-10}
31.69	13.379	13.340	6.153	3.283	1.887	1.145	0.723	0.477	0.319

4.3.3. Third section deformed radially

The affected parameters,

Capacitance to ground (C_{g3}) = 7.56 ×10^{-10}F. The inductance values as computed using FEM is given in Table 4.5.

Table 4.5 Self and mutual inductance in mH

L_{33}	M_{3-1}	M_{3-2}	M_{3-4}	M_{3-5}	M_{3-6}	M_{3-7}	M_{3-8}	M_{3-9}	M_{3-10}
31.678	6.153	13.369	13.378	6.155	3.284	1.887	1.144	0.731	0.476

4.3.4. Fourth section deformed radially

The affected parameters, Capacitance to ground (C_{g3}) = 6.94 ×10^{-10}FThe inductance values as computed using FEM is given in Table 4.6.

Table 4.6 Self and mutual inductance in mH

L_{44}	M_{4-1}	M_{4-2}	M_{4-3}	M_{4-5}	M_{4-6}	M_{4-7}	M_{4-8}	M_{4-9}	M_{4-10}
31.744	3.283	6.151	13.334	13.33	6.149	3.281	1.886	1.1579	0.7331

4.3.5. Fifth section deformed radially

The affected parameters, Capacitance to ground (C_{g5}) = 7.57 ×10^{-10}F. The inductance values as computed using FEM is given in Table 4.11.

Table 4.7 Self and mutual inductance in mH

L_{55}	M_{5-1}	M_{5-2}	M_{5-3}	M_{5-4}	M_{5-6}	M_{5-7}	M_{5-8}	M_{5-9}	M_{5-10}
31.71	1.889	3.286	6.155	13.361	13.34	6.151	3.281	1.906	1.1574

4.4. AXIAL DEFORMATION

The effects of axial forces may lead to axial overlap or shift of a portion of conductors over the other portion. This leads to axial deformation. Here, the axial overlap of half of the section over the other half is considered for the modeling of axial deformation using FEM as shown in Fig. 4.6. This is carried for five sections individually. The model of the axially deformed coil is shown in Fig. 4.5 developed using FEM. The affected parameters with axial deformation are series capacitance, ground capacitance and inductance.

Axial deformation occurs due to the action of axial forces on the winding conductors especially during short circuit situations. The effects of axial forces are tilting, bending, axial overlap of conductors, etc. The axial deformation of the helical winding is done by axially shifting half of a section conductors and overlapping them over the other half of the section as shown in Fig 4.6. This is done in FEM based software, MAGNET, for finding the values of inductance. The capacitance values are found using ELECNET. The ground capacitance, and series capacitance is same for all the deformed sections.

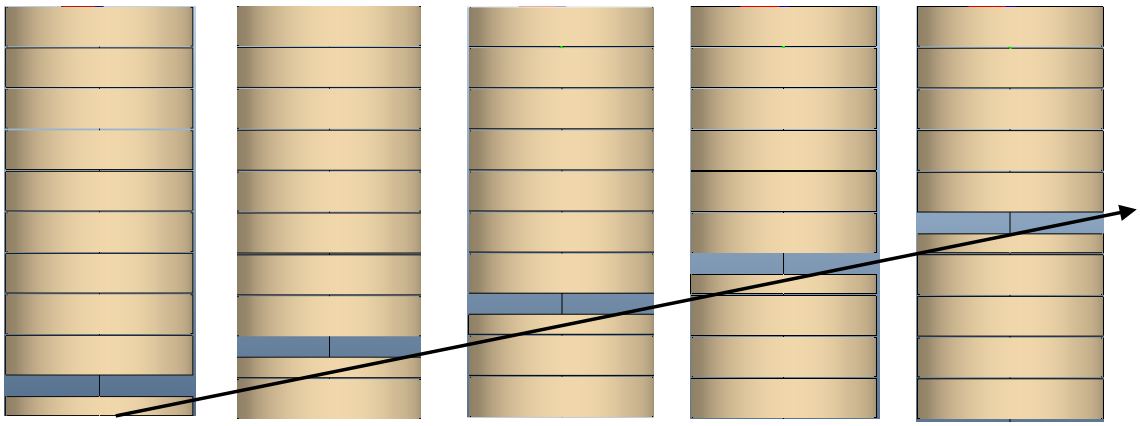

Fig. 4.5 Model designed using FEM to analyze axial deformations

Capacitance to ground, C_{gi}= 4.2× $10^{-10}F$

Series Capacitance, C_{si} = 5.87 × $10^{-12}F$

i=1, 2, 3, 4, 5

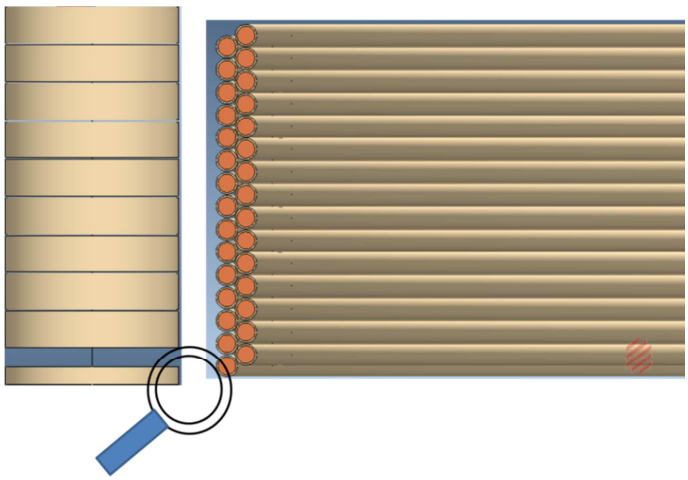

Fig. 4.6 Zoomed part of axial overlap portion for axial deformation

4.4.1. First section deformed axially

The model for first section deformed is shown in Fig. 4.3(a).The inductance values (in mH) are given in Table 4.8.

Table 4.8 Self and mutual inductance in mH

L_{11}	M''_{1-2}	M''_{1-3}	M''_{1-4}	M''_{1-5}	M''_{1-6}	M''_{1-7}	M''_{1-8}	M''_{1-9}	M''_{1-10}
36.8	10.173	4.831	2.607	1.508	0.919	0.585	0.384	0.258	0.177

4.4.2. Second section deformed axially

The inductance values (in mH) are given in Table 4.9.

Table 4.9 Self and mutual inductance in mH

L_{22}	M''_{2-1}	M''_{2-3}	M''_{2-4}	M''_{2-5}	M''_{2-6}	M''_{2-7}	M''_{2-8}	M''_{2-9}	M''_{2-10}
36.989	16.098	10.064	4.831	2.607	1.508	0.920	0.584	0.384	0.258

4.4.3. Third section deformed axially

The inductance values (in mH) are given in Table 4.10.

Table 4.10 Self and mutual inductance in mH

L_{33}	M''_{3-1}	M''_{3-2}	M''_{3-4}	M''_{3-5}	M''_{3-6}	M''_{3-7}	M''_{3-8}	M''_{3-9}	M''_{3-10}
36.9	0.25	15.96	10.078	4.833	2.608	1.508	0.920	0.585	0.384

4.4.4. Fourth section deformed axially

The inductance values are given in Table 4.11.

Table 4.11 Self and mutual inductance in mH

L_{44}	M''_{4-1}	M''_{4-2}	M''_{4-3}	M''_{4-5}	M''_{4-6}	M''_{4-7}	M''_{4-8}	M''_{4-9}	M''_{4-10}
36.8	3.502	6.714	15.94	10.078	4.833	2.608	1.508	0.920	0.584

4.4.5. Fifth section deformed axially

The inductance values are given in Table 4.12.

Table 4.12 Self and mutual inductance in mH

L_{55}	M''_{5-1}	M''_{5-2}	M''_{5-3}	M''_{5-4}	M''_{5-6}	M''_{5-7}	M''_{5-8}	M''_{5-9}	M''_{5-10}
36.8	3.502	6.714	15.94	10.078	4.833	2.608	1.508	0.920	0.584

4.5. CONCLUSION

The winding is modeled using finite element method (FEM) approach with radial and axial deformation. Such deformation is carried at five sections consecutively. As the parameters are affected by deformation in the winding, hence it is required to compute them after deformation. The affected parameters, the inductances and capacitances are calculated for all the five sections individually for both the deformed cases.

CHAPTER 5

LOCATION AND TYPE OF DEFORMATION

5.1. Introduction
5.2. SFRA application for deformation at different locations
5.3. SFRA results
5.4. Observations
5.5. Conclusion

5.1. INTRODUCTION

In the previous chapter, parameters affected during deformation of transformer winding such as capacitance and inductance are computed for healthy, radial and axial deformed cases using finite element method approach (FEM). These parameters are used to obtain SFRA graphs using MATLAB coding, for the healthy winding, which form a reference set for comparison with the SFRA graphs of deformed cases. The deviations in resonant frequency, peak input current and bandwidth are observed to be unique for each signature obtained for a particular location of a category of deformation.

5.2. SFRA application for deformation at different locations

The winding is radially deformed at five sections of the 10 section coil and the parameters are calculated using finite element method software. The changed values of the parameters are responsible for a modified fingerprint obtained for deformations at different locations. The SFRA obtained are compared with the reference fingerprint.

The affected parameters are ground capacitance, self and mutual inductance for the deformed section only. The SFRA is applied to the healthy winding by applying a constant magnitude sinusoidal voltage, 1volt for a frequency ranging from 50 Hz to 100 kHz and its frequency response is obtained. The frequency response is also obtained for deformed conditions. The healthy response is superimposed with the deformed responses. Fig. 5.1 shows the comparison of input current response for healthy and radially deformed sections at five locations. Similarly Fig. 5.2 and Fig. 5.3 shows the comparison of variation of resistance and reactance with frequency, respectively for all the radially deformed sections and healthy case. Similarly, Fig. 5.4 , Fig. 5.5, Fig. 5.6 shows the comparison of variation of input current, resistance and reactance respectively with frequency for axially deformed cases and healthy case.

Changes observed from the obtained SFRA plots after comparison with the reference plot are:

- Change in the shape of the curves
- Change in the resonant and anti-resonant frequencies
- Change in the magnitude of peak input current
- Change in the bandwidth of the curves

5.3. SFRA RESULTS

(a) Radial Deformation

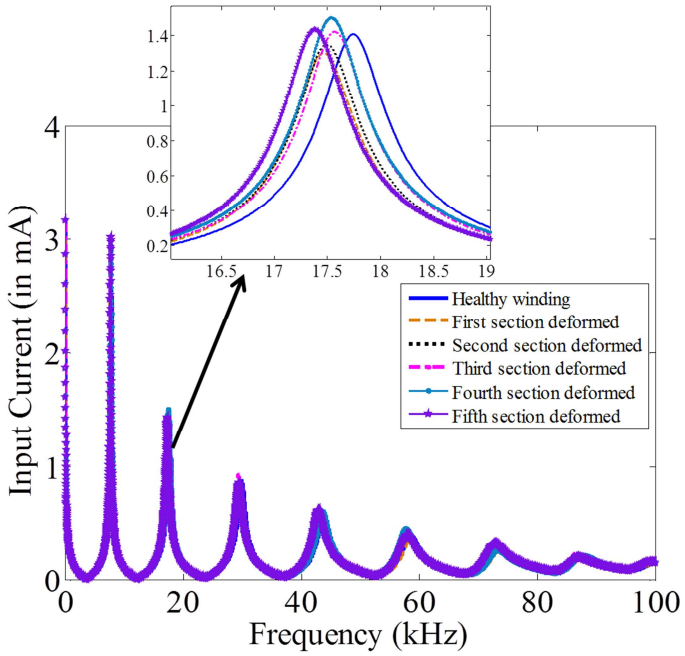

Fig. 5.1 Input current response with radial deformation

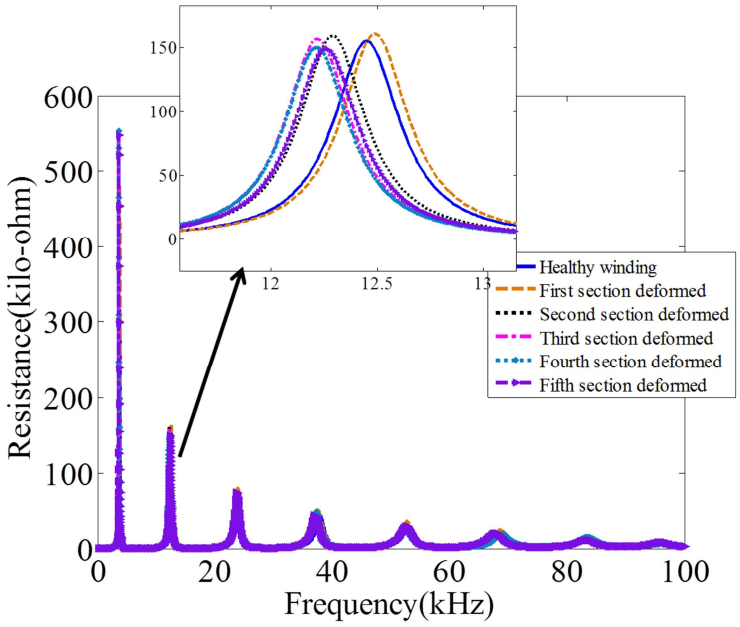

Fig. 5.2 Resistance plot with radial deformation

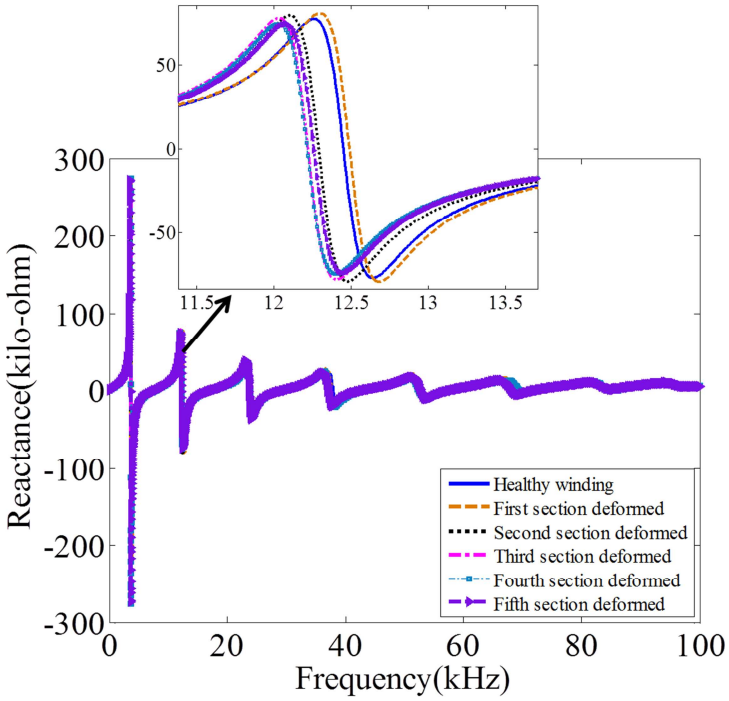

Fig. 5.3 Reactance plot with radial deformation

(b) Axial deformation

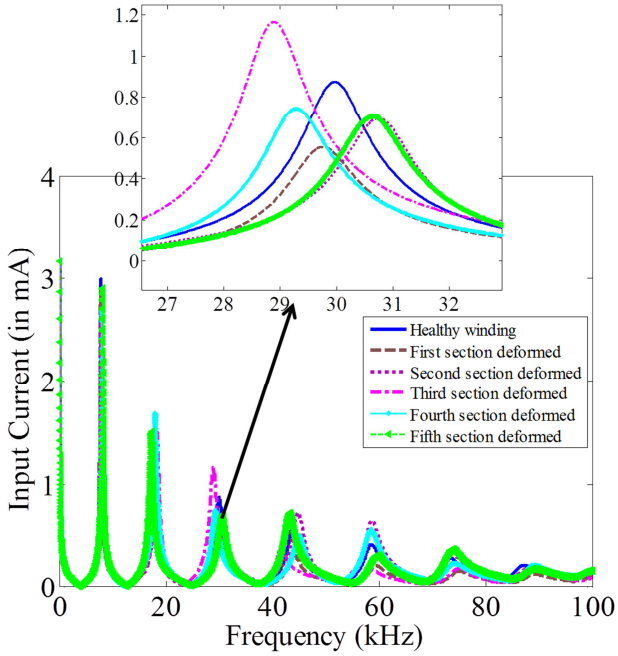

Fig. 5.4 Input current response with axial deformation

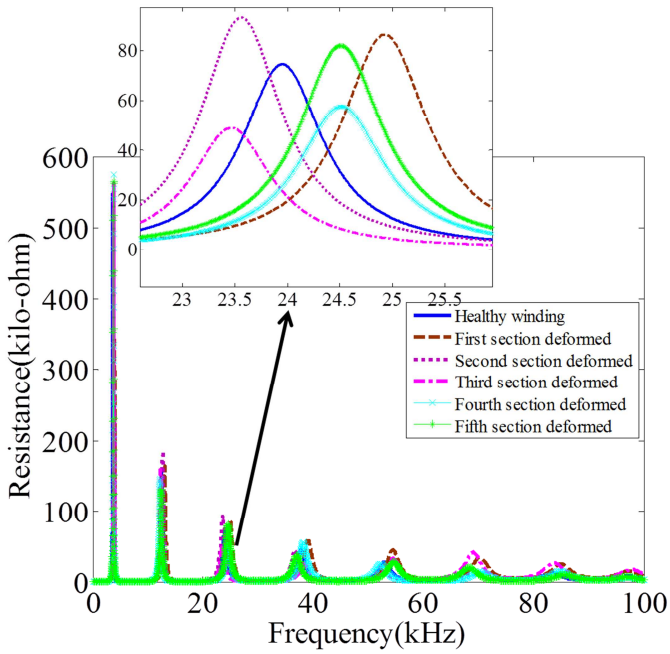

Fig. 5.5 Resistance plot for axial deformation

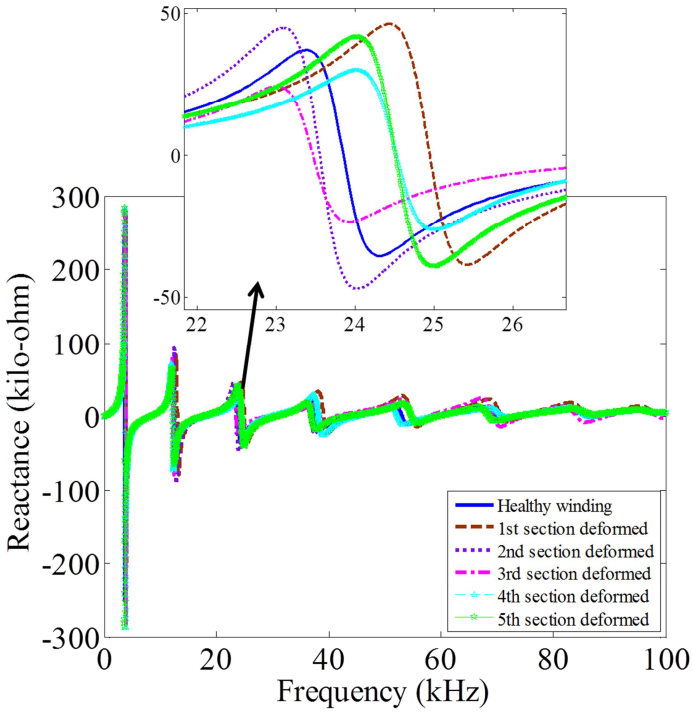

Fig. 5.6 Reactance plot for axial deformation

5.4. OBSERVATIONS

Table 5.1: Healthy winding

Harmonic Order	Resonant frequency, f_r (kHz)	Peak Current, I_r(mA)	Bandwidth, $B.W_r$.(kHz)
1st	7.84	3.02	0.02
2nd	17.70	1.39	0.50
3rd	29.65	0.88	1.00
4th	43.70	0.59	2.01
5th	58.70	0.42	2.60
6th	74.01	0.31	3.60
7th	88.40	0.20	4.90

The percentage of deviation is computed as given in (1). The measured indices for analyzing the deformations are resonant frequencies (f_r), peak input current (I_r) and bandwidth ($B.W_r$)

$$|\Delta d|\% = \frac{I_d - I_h}{I_h} \quad (1)$$

Where, $|\Delta d|\%$ is the percentage of deviation,

I_d is the measured index from the frequency response graph after applying deformation to the healthy winding,

I_h is the measured index from the frequency response graph of the healthy winding.

5.4.1. RADIAL DEFORMATION

Table 5.2: 1st section Radial deformation

Harmonic order	f_o (kHz)	$\|\Delta f_o\|$%	I_o(mA)	$\|\Delta I_o\|$%	B.W.(kHz)	|Δ B.W.|%
1st	7.70	1.78	2.94	2.52	0.02	31.90
2nd	17.46	1.30	1.31	6.89	0.60	19.98
3rd	29.45	0.67	0.78	11.60	1.20	19.60
4th	43.35	0.80	0.52	11.60	1.80	10.00
5th	58.50	0.34	0.36	7.96	2.70	3.85
6th	73.80	0.20	0.26	10.96	3.30	8.33
7th	87.70	0.79	0.18	9.18	4.67	4.69

Table 5.3: 2nd section radial deformation

Harmonic order	f_o (kHz)	$\|\Delta f_o\|$%	I_o(mA)	$\|\Delta I_o\|$%	B.W.(kHz)	|Δ B.W.|%
1st	7.71	1.65	2.95	2.22	0.02	35.99
2nd	17.49	1.19	1.35	3.29	0.60	19.98
3rd	29.55	0.67	0.86	2.27	1.10	9.98
4th	43.52	0.41	0.64	7.56	1.90	4.99
5th	58.48	0.34	0.46	7.72	2.40	7.69
6th	72.61	0.37	0.33	9.63	3.39	5.83
7th	87.70	0.79	0.21	0.96	5.01	2.24

Table 5.4: 3rd section radial deformation

Harmonic order	f_o (kHz)	$\|\Delta f_o\|$%	I_o(mA)	$\|\Delta I_o\|$%	B.W.(kHz)	|Δ B.W.|%
1st	7.74	1.28	2.94	7.70	0.02	23.98
2nd	17.57	0.73	1.42	1.93	0.56	11.97
3rd	29.38	1.24	0.92	4.77	1.10	9.98
4th	42.98	1.65	0.59	0.57	1.80	9.99
5th	58.02	2.55	0.39	7.72	2.61	0.50
6th	73.26	1.00	0.31	3.33	3.50	2.77
7th	86.90	1.69	0.23	13.04	4.70	4.08

Table 5.5: 4th section radial deformation

Harmonic order	f_o (kHz)	$\|\Delta f_o\|$%	I_o(mA)	$\|\Delta I_o\|$%	B.W.(kHz)	|Δ B.W.|%
1st	7.83	0.12	2.94	2.62	0.02	20.01
2nd	17.54	0.90	1.52	7.59	0.53	6.01
3rd	29.38	1.24	0.83	6.25	1.03	2.50
4th	43.68	1.65	0.61	1.93	1.80	9.98
5th	57.80	1.53	0.46	7.02	2.50	3.85
6th	73.40	0.81	0.26	13.33	3.70	2.77
7th	87.70	0.79	0.22	4.35	4.75	3.06

Table 5.6: 5th section radial deformation

Harmonic order	f_o (kHz)	$\|\Delta f_o\|$%	I_o(mA)	$\|\Delta I_o\|$%	B.W.(kHz)	|Δ B.W.|%
1st	7.79	0.64	3.02	0.09	0.02	20.01
2nd	17.38	1.81	1.44	2.79	0.60	19.52
3rd	29.53	0.74	0.86	2.61	1.15	14.65
4th	43.01	0.70	0.62	4.20	1.88	6.03
5th	58.01	1.19	0.40	6.32	2.80	7.61
6th	72.80	1.62	0.33	9.63	3.30	8.41
7th	87.01	1.58	0.19	5.79	4.70	4.12

The percentage of deviation in resonant frequencies is not so significant as it oscillates between 0.2% to approx. 2% for all the five sections radially deformed. The percentage of deviation is little higher for peak input current with a maximum of around 13%. However, the bandwidth has a greater deviation and hence more sensitive towards change in the physical configuration of the transformer winding. Hence, bandwidth can be used over frequency as an index for detecting radial deformation.

Further, the parameter values are calculated using finite element method (FEM) based software, these deviate from the values given in [2] by a 0.7% to a maximum 33%. Hence, the values calculated using FEM for deformed cases will also give approximate SFRA characteristics and percentage deviation from the reference characteristics, as expected for a real deformed case.

5.4.2. AXIAL DEFORMATION

Table 5.7: 1st section axial deformation

Harmonic order	f_o (kHz)	$\|\Delta f_o\|$%	I_o(mA)	$\|\Delta I_o\|$%	B.W.(kHz)	|Δ B.W.|%
1st	7.76	1.04	2.87	4.87	0.02	20.01
2nd	17.54	0.90	1.13	18.69	0.59	17.53
3rd	29.75	0.34	0.56	35.79	1.10	9.67
4th	43.96	0.59	0.31	47.06	2.25	12.50
5th	59.65	1.61	0.21	51.99	2.50	3.92
6th	75.26	1.68	0.15	50.36	3.80	5.47
7th	89.50	1.24	0.12	42.51	4.67	4.73

Table 5.8: 2nd section axial deformation

Harmonic order	f_o (kHz)	$\lvert\Delta f_o\rvert$%	I_o(mA)	$\lvert\Delta I_o\rvert$%	B.W.(kHz)	|Δ B.W.|%
1st	7.78	0.76	2.65	12.16	0.02	33.20
2nd	17.97	1.52	1.03	26.39	0.58	15.54
3rd	30.79	3.83	0.70	20.17	1.16	15.65
4th	44.86	2.65	0.72	22.26	1.60	20.01
5th	58.71	0.02	0.64	51.63	2.40	7.76
6th	73.39	0.84	0.33	11.29	3.70	2.69
7th	88.39	0.03	0.18	13.04	6.00	22.39

Table 5.9: 3rd section axial deformation

Harmonic order	f_o (kHz)	$\lvert\Delta f_o\rvert$%	I_o(mA)	$\lvert\Delta I_o\rvert$%	B.W.(kHz)	|Δ B.W.|%
1st	8.10	3.32	2.69	10.84	0.02	20.01
2nd	18.39	3.89	1.49	7.05	0.62	23.51
3rd	28.87	2.63	1.17	32.74	1.21	20.64
4th	41.64	4.71	0.36	39.21	1.67	16.65
5th	58.47	0.39	0.17	60.26	3.00	15.29
6th	75.13	1.51	0.18	40.56	3.30	8.41
7th	89.90	1.69	0.19	10.63	4.00	18.41

Table 5.10: 4th section axial deformation

Harmonic order	f_o (kHz)	$\lvert\Delta f_o\rvert$%	I_o(mA)	$\lvert\Delta I_o\rvert$%	B.W.(kHz)	|Δ B.W.|%
1st	8.05	2.67	2.69	10.83	0.02	12.60
2nd	17.96	1.44	1.69	21.06	0.57	14.74
3rd	29.29	1.23	0.74	15.56	1.20	19.64
4th	44.99	2.94	0.49	17.14	1.98	5.01
5th	58.42	0.47	0.55	29.50	2.48	3.92
6th	74.24	0.31	0.22	25.24	4.10	13.79
7th	89.03	0.68	0.20	0.96	5.02	1.99

Table 5.11: 5th section axial deformation

Harmonic order	f_o (kHz)	$\lvert\Delta f_o\rvert$%	I_o(mA)	$\lvert\Delta I_o\rvert$%	B.W.(kHz)	|Δ B.W.|%
1st	8.15	3.95	2.91	3.54	0.02	20.01
2nd	17.34	2.02	1.51	8.16	0.65	29.48
3rd	30.64	3.32	0.71	19.88	1.20	19.64
4th	43.25	1.03	0.72	21.17	1.87	6.25
5th	59.64	1.60	0.31	28.34	3.01	15.29
6th	73.76	0.34	0.36	20.63	3.51	2.85
7th	89.10	0.79	0.16	20.29	5.67	15.66

The percentage of deviation in peak input current for axial deformation shows a greater deviation than bandwidth from 3rd order onwards, unlike radial deformation

5.5. CONCLUSION

The modeling of deformed winding is performed using finite element method. The healthy and deformed cases are analyzed by applying sweep frequency response analysis (SFRA) and by using a comparative approach. The frequency response of the winding after deformation gives new resonant and anti-resonant frequencies. The shape of the curve changes and deviates from the response of the healthy winding. The aim of modeling deformations and applying SFRA at 5 sections sequentially is to find the probable location and type of deformation in an actual case. The computed parameters for the healthy winding, using finite element method (FEM) is found to agree with the parameter values given in [2] by a deviation 0f 0.64% to a maximum 33%. Hence it is assumed that the computed parameters for deformed cases will also agree with the actual changed parameter values given in Appendix I, with little deviation. Every sectional deformation whether radially or axially will give a different frequency response graph. The percentage of deviation in resonant frequencies, peak input current and bandwidth will also vary with harmonic orders and with location of deformation. Moreover, it is observed that the percentage of deviation in bandwidth is higher in case of radial deformation. While, the percentage of deviation in peak input current magnitude is higher from 3rd order onwards, as compared with bandwidth and resonant frequencies, in axial deformation analysis. In this way, by observing the percentage of deviation in the calculated indices, the location and type of deformation can be found as each section deformations gives a unique characteristic.

CHAPTER 6

CONCLUSION

5.1. Summary of work done
5.2. Future work

6.1. SUMMARY OF THE WORK DONE

The analysis of winding deformation is carried out by considering a benchmark winding which exhibits a similar high frequency behavior as a transformer. The winding is modeled using numerical modeling technique such as finite element method (FEM). The winding parameters such as series capacitance, ground capacitance, self and mutual inductance are computed using the FEM approach, at healthy condition. Further, the diagnostic method used here is sweep frequency response analysis (SFRA) which is a highly sensitive and powerful diagnostic technique. Using the parameters values and applying SFRA, fingerprint graph for the healthy winding is obtained. This is taken as reference plot for comparison with the unhealthy response corresponding to axial and radial deformation. For computing the modified parameters due to radial and axial deformation, the FEM modeling technique is used to model the deformation of the benchmark winding. Henceforth, the parameters computed are used to rebuild SFRA curves for the radial and axial deformation. The percentage of deviation in resonant frequencies, bandwidth and input current is observed in tabular form. It is observed from the tables that the percentage of deviation is highest in bandwidth for radial deformation while peak input current magnitude shows greater deviation for axial deformation. The location and type of deformation can be evaluated by the integrated use of FEM and SFRA plots.

6.2. FUTURE WORK

- In this thesis, an offline diagnosis of deformation is only carried out using FEM modeling approach with SFRA application using MATLAB code. However, an onsite diagnosis of deformation at different locations of transformer winding using SFRA can be carried out.
- Experimental verification of the diagnosis at different locations using an experimental coil having similar features as the single layer helical winding.

APPENDIX I

A.1. Parameter values for 10 section model

C_g	=	$8.5 \times 10^{-10} F$	C_s	=	$3.4 \times 10^{-12} F$
R_g	=	$2.1 \times 10^{11} \Omega$	R_s	=	$1.65 \times 10^{5} \Omega$
r_s	=	$22.6\ \Omega$			
L_{11}	=	29.186 mH	M_{1-6}	=	1.242 mH
M_{1-2}	=	13.620 mH	M_{1-7}	=	0.817 mH
M_{1-3}	=	6.228 mH	M_{1-8}	=	0.551 mH
M_{1-4}	=	3.379 mH	M_{1-9}	=	0.405 mH
M_{1-5}	=	1.981 mH	M_{1-10}	=	0.292 mH

B.1. Parameter values for 20 section model

C_g	=	$4.25 \times 10^{-10} F$	C_s	=	$6.8 \times 10^{-12} F$
R_g	=	$4.2 \times 10^{11} \Omega$	R_s	=	$8.25 \times 10^{4} \Omega$
r_s	=	$11.3\ \Omega$			
L_{11}	=	9.308 mH	M_{1-11}	=	0.309 mH
M_{1-2}	=	5.304 mH	M_{1-12}	=	0.242 mH
M_{1-3}	=	3.099 mH	M_{1-13}	=	0.206 mH
M_{1-4}	=	2.116 mH	M_{1-14}	=	0.163 mH
M_{1-5}	=	1.505 mH	M_{1-15}	=	0.134 mH
M_{1-6}	=	1.101 mH	M_{1-16}	=	0.119 mH
M_{1-7}	=	0.825 mH	M_{1-17}	=	0.100 mH
M_{1-8}	=	0.629 mH	M_{1-18}	=	0.085 mH
M_{1-9}	=	0.485 mH	M_{1-19}	=	0.072 mH
M_{1-10}	=	0.382 mH	M_{1-20}	=	0.062 mH

APPENDIX II

MATLAB CODE FOR SFRA OF HEALTHY WINDING

```
clear
sections = 10;
elements = 6*sections-2;
  Z11=[ ];
for f=50:50:100e3
w=2*pi*f;
%%%%% L11  M1-2  M1-3  M1-4   M1-5  M1-6   M1-7  M1-8  M1-9    M1-10
Mdata=[28.8 12.87 5.731 3.012 1.7126 1.0302 0.649 0.422 0.2848 0.19427]*j*w*1e-3;
Cdata=[4.2e-12 7.7264e-10];
yprimitive=zeros(elements,elements);
XL=w*mdata(1,1);
YCs=w*Cdata(1,1);
XCs=1/YCs;
Rdata=[1.65e5 22.6 2.1e11];
YCg=w*Cdata(1,2);
XCg=1/YCg;
zself=[];
for i=1:9
      zself=[zself Rdata -j*XCs -j*XCg];
end
zprim1=diag(zself);
z1=[1.65e5 22.6 -j*XCs];
z2=diag(z1);
zf=[zprim1,zeros(45,3);zeros(3,45),z2];
for a=1:10
       for k=1:9
           for i=1:10
        if abs(k+1-a)==i
                    Xlm(a,k+1)=mdata(1,i+1);
                    Xlm(k+1,a)=Xlm(a,k+1);
        end
           end
       end
end
      for a=1:10
         Xlm(a,a)=mdata(1,1);
      end
```

```
yprimitive=[inv(zf) zeros(48,10); zeros(10,48) inv(Xlm)];
 A1=[];
 B1=[];
 D1=[];
 for n=0:8
    a=5*n+1;
    b=a+1;
    c=b+1;
    d=c+1;
    e=d+1;
    c1=2*n+1;
    c2=c1+1;
    c3=c2+1;
    A1=[A1 [a b c d e a b d]];
    B1=[B1 [c1 c2 c3 c1 c3 c3 c3 c3]];
    D1=[D1 [1 1 1 1 1 -1 -1 -1]];
 end
     A=sparse(A1,B1,D1,48,20);
A(46,19)=1;
A(47,20)=1;
A(48,19)=1;
   S1=[];
   S2=[];
   S3=[];
   for n=0:9
      a=n+1;
      b=2*n+1;
      c=b+1;
      S1=[S1 [a a]];
      S2=[S2 [b c]];
      S3=[S3 [1 -1]];
   end
   S=sparse(S1,S2,S3,10,20);
   Afinal=[A;S];          %incidence matrix
   Ybus=Afinal'*yprimitive*Afinal;   %Bus admittance matrix
   Zbus=inv(Ybus);
   Z11=[Z11 Zbus(1,1)];
end
f=50:50:100e3;
t=abs(Z11);
```

```
Iwd=1./t;
plot(f*1e-3,Iwd*1e3);            %Input Current Plot
figure;
plot(f*1e-3,real(Z11)*1e-3,'r');          %Resistance plot
hold on;
xw=imag(Z11);
plot(f*1e-3,xw*1e-3);            %Reactance Plot
hold off;
```

REFERENCES

[1] P. A. Abetti and F. J. Maginniss, "Natural Frequencies of Coils and Windings Determined by Equivalent Circuit," *IEEE Trans. On Power App. Syst.*, pp. 495-503, June 1953

[2] R. C. Degeneff, "A General Method of Determining Resonances in Transformer Windings," *IEEE Trans. On Power App. Syst*., vol. 96, no. 2, pp. 423-430, Mar./Apr. 1977.

[3] E. Billig, "Mechanical Stresses in Transformer Windings", Electrical Engineers - Part II: Power Engineering, *IEEE journals and magazines*, vol. 93 , No. 33, 1946.

[4] L.V. Bewley, J. H. Hagenguth and F. R. Jackson, JR., "Methods of Determining Natural Frequencies in Coils and Windings," *AIEE Trans*., vol. 60, pp. 1145-1150, 1941.

[5] P. A. Abetti and F. J. Maginniss, "Fundamental Oscillations of Coils and Windings," *IEEE Trans. On Power App. Syst*., pp. 1-10, Feb. 1954.

[6] W. Lech, L. Tyminski, "Detecting Transformer Winding Damage-The Low Voltage Impulse Method", *Electrical Review*, No. 21, Vol.179, November 1966, pp 768-772, (ERA Translation).

[7] K. Ragavan and L. Satish, "An Efficient Method to Compute Transfer Function of a Transformer from its Equivalent Circuit," *IEEE Trans. On Power Delivery*, vol. 20, no. 2, April 2005.

[8] P. I. Fergestad and T. Henriksen, "Transient Oscillations in Multiwinding Transformers," *IEEE Trans. Power App. Syst.*,vol. 93, no. 2, pp. 500-509,

[9] S. A. Ryder, "Diagnosing Transformer Faults using Frequency Response Analysis," *IEEE Electrical Insulation Magazine*, vol.19, no.2, pp. 16-22, 2003.

[10] S. Gopalakrishna, J Joseph, and V. Jayashankar, "On the Use of Concurrent High Frequency Excitation during a Short Circuit Test in a Power Transformer," *International Instrumentation and Measurement Technology Conference*, pp.1258-1261, May 2009.

[11] S. V. Kulkarni, and S. A. Khaparde, "Transformer Engineering Design and Practice", New York: Marcel Dekker, 2004.

[12] F. W. Grover, *Inductance Calculations: Working Formulas and Tables*, Dover Publications Inc., New York, 1946.

[13] S.Gopalakrishna, M.K.Ilampoornan and V.Jayashankar, "Sensitive Method for Detection of Winding Deformation during Short Circuit Test", *International Symposium on Electrical Insulating Materials*, pp. 167-170, Japan, September 2008.

[14] Christain, J.,and K. Feser (2004) , "Procedures for detecting winding displacement in power transformers by transfer function method", *IEEE Transactions on Power Delivery.*, vol.19, no.1, pp. 214-219.

[15] E.P.Dick and C.C.Erven. "Transformer diagnostic testing by frequency analysis*", IEEE Trans. on Power Apparatus and Systems*, 1978, vol. 97, pp. 2144-2153

[16] E. Rahimpour, J. Christian, K. Feser, and H. Mohseni, "Transfer function method to diagnose axial displacement and radial deformation of transformer windings," *IEEE Trans. Power Del.* ,vol. 18, no. 2, pp.493–505, Apr. 2003.

[17] N. Abeywickrama, Y. Serdyuk, and S. Gubanski, "High-frequency modeling of power transformers for use in frequency response analysis(FRA)," *IEEE Trans. Power Del.*, vol. 23, no. 4, pp. 2042–2049, Oct.2008.

[18] Jawad Faiz, Bashir Mahdi Ebrahimi, and Tahere Noori, "Three- and Two-Dimensional Finite-Element Computation of Inrush Current and Short-Circuit Electromagnetic Forces on Windings of a Three-Phase Core-Type Power Transformer", *IEEE Transactions on Magnetics*, vol. 44, no. 5, May 2008.

[19] Asif Islam, Shahidul Islam Khan, Aminul Hoque, "Detection of Mechanical Deformation in Old Aged Power Transformer Using Cross Correlation Co-Efficient Analysis Method", *Energy and Power engineering*, vol. 3, pp. 585-591, 2011.

[20] P.M. Nirgude, D. Ashokraju, A.D. Rajkumar, B.P. Singh, "Application of numerical evaluation techniques for interpreting frequency response measurements in power transformers", *IET Science, Measurement and Technology*, 2008, vol. 2, no. 5, pp. 275–285

[21] S. Tenbohlen and S. A. Ryder, "Making Frequency Response Analysis Measurements: A Comparison of the Swept Frequency and Low Voltage Impulse Methods", *XIIIth International Symposium on High Voltage Engineering, Netrherlands* , 2008.

[22] P. M. Joshi and S. V. Kulkarni, Transformer Winding diagnostics using Deformation Coefficients", *Power and Energy Society General Meeting - Conversion and Delivery of Electrical Energy in the 21st Century*, 2008

[23] Steven D. Mitchell and James S. Welsh, "Modeling Power Transformers to Support the Interpretation of Frequency-Response Analysis", *IEEE Transactions on Power Delivery*, vol. 26, no. 4, October 2011.

[24] J.R. Secue and E. Mombello, "Sweep frequency response analysis (SFRA) for the assessment of winding displacements and deformation in power transformers", *Electric Power Systems Research* , vol. 78, pp.1119–1128, 2008.

[25] S. Gopalakrishna, Kishore Kumar, Boby George, and V. Jayashankar**, "**Design margin for short circuit withstand capability in large power transformer", Proceedings of *8th International Power Engineering Conference (IPEC-2007)*, pp. 1732-1737, December, 2007.

[26] T. D. Rybel , " Apparatus for on-line power transformer winding monitoring using bushing tap injection", *IEEE Trans. Power Delivery*, vol. 24, no. 3, pp. 996-1003, July 2009.

[27] T. Leibfried and K. Feser, "Monitoring of power transformers using the transfer function method," *IEEE Trans. Power Delivery*, vol. 14, pp. 1333–1341, Oct. 1999.

[28] K. Feser, J. Christian, C. Neumann, U. Sundermann, T. Leibfried, A. Kachler, andM. Loppacher, "The transfer function method for detection of winding displacements on power transformers after transport, shorcircuit or 30 years of service," in CIGRE 12/33-04, 2000.

[29] J. Christian, K. Feser, U. Sundermann, and T. Leibfried, "Diagnostic of power transformers by using the transfer function method," *in Proc. 11th Int. Symp. High Voltage Eng.*, vol. 1, pp. 37–40, London, U.K., Aug. 1999.

[30] P. T. M. Vaessen, "Transformer model for high frequencies," *IEEE Trans. Power Delivery*, vol. 3, pp. 1761–1768, Oct. 1988.

[31] A. Morched, L. Marti, and J. Ottewangers, "A high frequency transformer model for the EMTP," IEEE Trans. Power Delivery, vol. 8, pp. 1615–1626, July 1993.

[32] Y. Shibuya, S. Fujita, and N. Hosokawa, "Analysis of very fast transient overvoltage in transformer winding," *Proc. Inst. Elect. Eng..-Gene Transm. Distrib.*, vol. 144, no. 5, pp. 461–468, Sept. 1997.

[33] S. Gopalakrishna, V. Jayashankar, V. Jagadeesh Kumar and N. Madhu Mohan, "Online assessment of winding deformation based on optimised excitation", *International Workshop on Applied Measurements for Power Systems (AMPS–2010)*, pp. 84-89, Aachen, Germany, Sep. 2010.

[34] S. Gopalakrishna, *Ph.D. Thesis*, Dept. of Electrical Engineering, Indian Institute of Technology Madras, Chennai, India, 2010